THE ACS FORNAX CLUSTER SURVEY. V. MEASUREMENT AND RECALIBRATION OF SURFACE BRIGHTNESS FLUCTUATIONS AND A PRECISE VALUE OF THE FORNAX–VIRGO RELATIVE DISTANCE[*]

JOHN P. BLAKESLEE[1,2], ANDRÉS JORDÁN[3,4], SIMONA MEI[5,6], PATRICK CÔTÉ[1], LAURA FERRARESE[1], LEOPOLDO INFANTE[4],
ERIC W. PENG[7], JOHN L. TONRY[8], AND MICHAEL J. WEST[9]

[1] Dominion Astrophysical Observatory, Herzberg Institute of Astrophysics, National Research Council of Canada, Victoria, BC V9E 2E7, Canada;
John.Blakeslee@nrc.ca
[2] Department of Physics and Astronomy, Washington State University, Pullman, WA 99163-2814, USA
[3] Harvard-Smithsonian Center for Astrophysics, Cambridge, MA 02138, USA
[4] Departamento de Astronomía y Astrofísica, Pontificia Universidad Católica de Chile, Santiago 22, Chile
[5] University of Paris Denis Diderot, 75205 Paris Cedex 13, France
[6] GEPI, Observatoire de Paris, Section de Meudon, 5 Place J. Janssen, 92195 Meudon Cedex, France
[7] Department of Astronomy, Peking University, Beijing 100871, China
[8] Institute for Astronomy, University of Hawaii, Honolulu, HI 96822, USA
[9] European Southern Observatory, Alonso de Cordova 3107, Vitacura, Santiago, Chile

ABSTRACT

We present $(g_{475}-z_{850})$ color and z_{850}-band surface brightness fluctuations (SBFs) measurements for 43 early-type galaxies in the Fornax cluster imaged with the *Hubble Space Telescope* Advanced Camera for Surveys. These are combined with our earlier measurements for Virgo cluster galaxies to derive a revised, nonlinear calibration of the z_{850}-band SBF absolute magnitude $\overline{M}_z$ as a function of $(g_{475}-z_{850})$ color, valid for the AB color range $0.8 < (g_{475}-z_{850}) < 1.6$. In all, we tabulate recalibrated SBF distances for 134 galaxies in Virgo, Fornax, the Virgo W' group, and NGC 4697 in the Virgo Southern Extension. The calibration procedure yields a highly precise relative distance modulus for Fornax with respect to Virgo of $\Delta(m - M)_{FV} = 0.42 \pm 0.03$ mag, or a distance ratio $d_F/d_V = 1.214 \pm 0.017$. The resulting Fornax distance modulus is $(m - M)_{\rm For} = 31.51 \pm 0.03 \pm 0.15$ mag, corresponding to $d_F = 20.0 \pm 0.3 \pm 1.4$ Mpc, where the second set of error bars reflects the total systematic uncertainty from our assumed Virgo distance of 16.5 Mpc. The rms distance scatter for the early-type Fornax cluster galaxies is $\sigma_d = 0.49^{+0.11}_{-0.15}$ Mpc, or a total line-of-sight depth of $2.0^{+0.4}_{-0.6}$ Mpc, consistent with its compact appearance on the sky. This translates to a depth scatter smaller than the intrinsic, or "cosmic," scatter $\sigma_{\rm cos}$ in the SBF calibration, unlike the case for the larger Virgo cluster. As a result, we are able to place the first tight constraints on the value of $\sigma_{\rm cos}$. We find $\sigma_{\rm cos} = 0.06 \pm 0.01$ mag, with a firm upper limit of $\sigma_{\rm cos} < 0.08$ mag, for the subsample of galaxies with $(g_{475}-z_{850}) > 1.02$, but it is about twice as large for bluer galaxies. We also present an alternative SBF calibration based on the "fluctuation count" parameter $\overline{N} = \overline{m} - m_{\rm tot}$, a proxy for galaxy mass. This gives a consistent relative distance but with larger intrinsic scatter, and we adopt the result from the calibration on $(g_{475}-z_{850})$ because of its basis in stellar population properties alone. Finally, we find no evidence for systematic trends of the galaxy distances with position or velocity (e.g., no current infall); the Fornax cluster appears both compact and well virialized.

Key words: galaxies: clusters: individual (Fornax, Virgo) – galaxies: distances and redshifts – galaxies: elliptical and lenticular, cD – large-scale structure of universe

Online-only material: color figures

1. INTRODUCTION

It is now more than 20 years since Tonry & Schneider (1988) first quantified the surface brightness fluctuations (SBFs) method for determining extragalactic distances. That paper envisioned SBF potentially being used to measure distances to elliptical galaxies out to 20 Mpc from the ground and being calibrated from stellar evolution models tied to Galactic clusters with distances from main-sequence fitting. Tonry & Scheider noted that the absolute fluctuation magnitude $\overline{M}$ would vary with the age and metallicity of a stellar population, but they predicted that the mean color of a galaxy could be used to constrain $\overline{M}$ to within 0.4 mag, allowing galaxy distance measurements accurate to at least ∼20%.

The first major application of the fully developed SBF method was by Tonry et al. (1990), who applied it to a sample of Virgo cluster galaxies in the *VRI* bandpasses. They calibrated the $\overline{M}$ zero point from measurements in M31 and M32, assuming the Cepheid distance to M31. The depth of Virgo, including the unexpected discovery that the giant elliptical NGC 4365 apparently lay in the background, precluded a good determination of the dependence of $\overline{M}$ on stellar population. Soon afterward, observations of galaxies in the compact Fornax cluster provided the first fully empirical SBF calibration, determining $\overline{M}_I$ as a function of galaxy $(V-I)$ color (Tonry 1991). The ensuing ground-based SBF Survey of Galaxy Distances (Tonry et al. 1997, 2001) determined distances to some 300 early-type galaxies and spiral bulges. It also uncovered and corrected various problems with the photometric consistency of the earlier observations. The median error in distance modulus from the ground-based SBF survey was

0.22 mag, or 10%, including an estimated "cosmic scatter" of 0.06 mag intrinsic to the $\overline{M}$–$(V-I)$ relation (Tonry et al. 2000). This level of accuracy was a substantial improvement over previous large surveys using other distance indicators.

At the same time, SBF measurements with the repaired *Hubble Space Telescope* (*HST*) gave the first hints of the enormous potential of the method with space-based resolution (Ajhar et al. 1997, 2001; Pahre et al. 1999; Neilsen & Tsvetanov 2000). However, the characteristics of WFPC2 (small area of the PC chip, severe undersampling of the WF chips, modest quantum efficiency) limited the use of this instrument for SBF observations. For further details on the first decade of SBF studies, see the review by Blakeslee et al. (1999). For information on applications of the method using NICMOS on *HST*, including stellar population effects and the unique systematics of that detector, see Jensen et al. (2001, 2003).

More recently, there has been renewed interest in ground-based SBF studies, mainly targeting dwarf galaxies in several nearby groups using large-aperture telescopes (e.g., Mieske et al. 2003, 2006; Jerjen 2003; Jerjen et al. 2004; Dunn & Jerjen 2006). There has also been significant theoretical effort to predict the behavior of SBF magnitudes in various bandpasses as a function of stellar population (Liu et al. 2000; Blakeslee et al. 2001b; Mei et al. 2001; Cantiello et al. 2003; Mouhcine et al. 2005; Raimondo et al. 2005; Marín-Franch & Aparicio 2006; Lee et al. 2007; Cerviño et al. 2008). Additionally, SBF measurements in Magellanic Cloud star clusters of varying ages (González et al. 2004; González-Lópezlira et al. 2005; Raimondo et al. 2005) have provided important new tests and calibration data for stellar population synthesis modeling. These studies show that some discrepancies remain between observations and models, as well as among the different model predictions, particularly in the near-IR where thermally pulsing AGB stars can have a major effect on SBF magnitudes. Much work remains to be done to resolve these outstanding issues.

The full promise of the optical SBF method was finally brought to fruition with the installation of the Advanced Camera for Surveys (ACS) on board *HST*. The ACS Wide Field Channel (WFC) samples the point-spread function (PSF) with a resolution comparable to the WFPC2 planetary camera CCD, but over a much larger $\sim 3\farcm3 \times 3\farcm3$ field and with about 5 times the throughput at the wavelengths typically used for SBF analyses. SBF investigations with ACS/WFC in the F814W bandpass (most similar to the *I* band) include the first studies of large samples of high signal-to-noise radial SBF gradients in early-type galaxies (Cantiello et al. 2005, 2007a), the first optical SBF distance measurements out to ~ 100 Mpc or beyond (Biscardi et al. 2008), and a precise distance to a peculiar gas-rich S0 galaxy in the Dorado group (Barber Degraaff et al. 2007). The ACS/WFC has also afforded the first samples of reliable *B*-band (F435W) SBF measurements beyond the Local Group (Cantiello et al. 2007b), which are useful for stellar population work.

However, the potential of the SBF method when combined with a large-format, high-throughput, well-sampled, space-based imager has been most spectacularly demonstrated by its application in the F850LP bandpass (hereafter z_{850}) as part of the ACS Virgo Cluster Survey (ACSVCS; Côté et al. 2004, hereafter ACSVCS-I), a two-band imaging survey of 100 early-type galaxies in the Virgo cluster with the ACS/WFC. The data analysis and calibration of the z_{850}-band SBF method are described in detail by Mei et al. (2005a, 2005b, hereafter ACSVCS-IV, ACSVCS-V). The precision of the ACSVCS SBF

distances is about 3 times better than for the same galaxies as measured in the ground-based *I*-band survey, and it has been possible to measure distances for about 3 times as many Virgo galaxies. As a result, the ACSVCS SBF measurements provide the first clear resolution of the three-dimensional distribution of the early-type galaxy population in Virgo (Mei et al. 2007, hereafter ACSVCS-XIII).

The ACS Fornax Cluster Survey (ACSFCS; Jordán et al. 2007, hereafter ACSFCS-I) was designed as a companion survey to the ACSVCS, with similar goals and observing strategy, but targeting 43 galaxies in the Fornax cluster, the next nearest cluster after Virgo. Other papers in this series deal with the central brightness profiles in Fornax and Virgo early-type galaxies and with galaxy scaling relations (Côté et al. 2007; P. Côté 2009, in preparation). Future works will address isophotal analysis of galaxy structure (L. Ferrarese et al. 2009, in preparation), as well as the properties of the globular cluster populations. As discussed in ACSFCS-I, Fornax is considerably more compact and regular in shape than Virgo, with a central density of galaxies about twice as large but a total mass nearly an order of magnitude lower. The two clusters therefore make a useful comparison for investigations of environmental effects on galaxies, a prime motivation for the ACSFCS. The compact structure of Fornax has also made it a frequent target for distance scale studies (e.g., Tonry 1991; Madore et al. 1998; Dunn & Jerjen 2006), but different methods often disagree regarding the relative distance between the Fornax and Virgo clusters (e.g., Ferrarese et al. 2000).

An important goal of the ACSFCS was therefore to refine the z_{850} SBF calibration and take advantage of the homogeneity of the two data sets and small internal scatter of the method to determine a precise relative distance between Virgo and Fornax. Knowledge of the relative distance is essential for making accurate comparisons between the galaxy and star cluster properties in these two archetypal clusters. Here, we present the SBF analysis of the 43 galaxies observed in the ACSFCS. The following section summarizes the observations and data analysis. Section 3 details our SBF and galaxy $(g_{475}-z_{850})$ color measurements and infers the dependence of F850LP SBF on color from the Fornax data alone. Section 4 combines these measurements with our earlier ACSVCS SBF measurements to determine a calibration from the full sample of galaxies and a precise estimate of the relative distance modulus between the two clusters. In Section 5, we compare our new measurements to literature values, examine the structural properties of Fornax, and discuss an alternative SBF calibration based on the parameter $\overline{N}$, the difference between the SBF magnitude and the total magnitude of the galaxy. The final section provides a summary of our results.

2. OBSERVATIONS AND REDUCTIONS

A complete sample of 44 Fornax cluster galaxies was initially targeted as part of the Cycle 13 *HST* GO program 10217, the ACSFCS. Of these, 42 constitute a complete sample of early-type galaxies with total *B*-band magnitudes $B_T \leqslant 15.5$ from the Fornax Cluster Catalogue (FCC) of Ferguson (1989). The two other targets, NGC 1340 and IC 2006, are bright early-type galaxies just outside the FCC survey area. All of the targets are located within $3\fdg25$ of the cD galaxy NGC 1399, or about 1.1 Mpc for $d \approx 20$ Mpc. However, because of a guide star acquisition failure, the bright elliptical NGC 1379 (FCC 161) was not observed, leaving a total sample of 43 galaxies.

Full details on the observational program, including motivations, design specifications, sample properties, observing log, and basic image processing methods, are given in ACSFCS-I. Further information on the data reduction techniques is given by Jordán et al. (2004, hereafter ACSVCS-II). Briefly, each galaxy was observed for one orbit, including two exposures totaling 760 s in the F475W (g_{475}) bandpass and three exposures totaling 1220 s in F850LP (z_{850}). The exposures were dithered; we used the alignment routines in the Apsis package (Blakeslee et al. 2003) to determine offsets, then combined the images using the Multidrizzle (Koekemoer et al. 2002) interface to the Drizzle (Fruchter & Hook 2002) image resampling software. We use the Lanczos3 interpolation kernel to reduce the small-scale noise correlations. As discussed in detail by ACSVCS-IV, this is an important consideration for obtaining accurate SBF power spectrum measurements.

The data were photometrically calibrated using the F475W and F850LP zero points from Sirianni et al. (2005). Although small refinements to these zero points are available from STScI on the ACS data analysis Web site,[10] we use the published values to retain consistency with our earlier ACSVCS and ACSFCS publications. The revisions to the absolute sensitivity of the ACS detectors have no bearing on the internally calibrated SBF results of the present work. All of the observations were completed before the change of the ACS/WFC operating temperature in 2007 July and consequent change in photometric sensitivity. The photometry was corrected for Galactic extinction using the dust maps of Schlegel et al. (1998) with the extinction ratios adopted by ACSVCS-II from Sirianni et al. (2005).

ACSVCS-IV outlined the general steps for measuring the SBF amplitude from the power spectrum of a galaxy image and used realistic image simulations to demonstrate that our SBF analysis of the ACS/WFC data produced accurate results. The analysis is performed on the F850LP image to measure the SBF magnitude $\overline{z}_{850}$ because the SBF is bright and well behaved in this bandpass (ACSVCS-I, ACSVCS-V). It is too faint to measure reliably in our F475W images; however, we use both images to measure the galaxy ($g_{475}-z_{850}$) color and calibrate the variation of $\overline{z}_{850}$ with stellar population, as described in detail below. The basic SBF method is the same as described in many previous works (e.g., Tonry et al. 1990; Jacoby et al. 1992; Jensen et al. 1998; Blakeslee et al. 1999; Mei et al. 2003). It involves constructing a two-dimensional model of the galaxy light, subtracting the model and sky from the image, detecting sources (stars, globular clusters, background galaxies), masking the sources and any dust or other irregular features in the galaxy-subtracted "residual image," measuring the amplitude of the power spectra in different regions of the masked residual image, correcting the measurements for contamination from undetected sources, and combining the results to obtain the average SBF magnitude.

Specific details on the analysis regions, masking, corrections, etc., for the ACSVCS data are given by ACSVCS-V. The method for identifying regions affected by dust is described in detail by Ferrarese et al. (2006, hereafter ACSVCS-VI). Details on the two-dimensional galaxy fitting for the present sample are provided in ACSFCS-I. In general, we followed the same SBF reduction procedures as in the ACSVCS in order to ensure homogeneity between the two surveys. Where the analysis was modified, mainly for the sake of streamlining, we verified that the changes caused no systematic differences in the results.

The following section describes our SBF magnitudes and color measurements, noting any areas where the procedures have been revised from our earlier work.

3. SBF AND COLOR MEASUREMENTS

We measure the power spectrum of the masked residual image in a series of contiguous, concentric annuli with inner radii of $1\farcs6$, $3\farcs2$, $6\farcs4$, $12\farcs8$, $19\farcs2$, $25\farcs6$, $32''$, and $38\farcs4$, the same annuli as used for the ACSVCS measurements. The galaxy center is determined from our isophotal modeling. In many cases, the innermost one or two annuli are omitted because they suffer from poor model residuals or significant dust contamination. In addition, we only use annuli where the mean galaxy surface brightness is at least 60% of the sky level, which effectively sets the outermost radius for most galaxies (except the giants, for which the galaxy surface brightness is significantly above the sky level for all annuli). This limit is slightly more conservative than the 50% value quoted in ACSVCS-V, but the small change has no significant systematic effect on the results. The median number of annuli analyzed per galaxy is 5 (the average is 5.2).

The power spectrum of each annulus in each galaxy is azimuthally averaged and modeled as a linear combination of two components:

$$P(k) = P_0 \times E(k) + P_1, \qquad (1)$$

where P_0 and P_1 are constants and $E(k)$ is the "expectation power spectrum," which is the convolution of the power spectrum of the normalized PSF with the mask function of the annular region. As noted in the previous section, ACSVCS-IV demonstrated that the power spectra are not significantly modified by pixel correlation induced by our interpolation kernel. The coefficient P_0 represents the signal we are trying to measure, while P_1 includes shot noise, read noise, and any other sources of variance that are not convolved with the PSF.

We used two different robust fitting routines available from the IDL Astronomy Library[11] to determine the coefficients in Equation (1). These were the least absolute deviation procedure LADFIT used in ACSVCS-V, and an iterative rejection procedure using bisquare weights called ROBUST_POLY_FIT. The median difference in the final results using these two different fitting methods was 0.006 mag, with an rms scatter in the differences of 0.034 mag. Because there was no significant systematic difference, we averaged the results from the two sets of fits and included half the difference in quadrature in our error estimation.

The final step in determining the SBF signal for each annulus is to estimate the residual variance contamination P_r due to undetected sources and subtract it from P_0 to derive the variance due to SBF: $P_{\mathrm{SBF}} = P_0 - P_r$. This is normalized by the galaxy surface brightness and converted to the SBF magnitude $\overline{z}_{850}$. We used the same software and followed the identical procedures as in ACSVCS-V to estimate the background variances based on the expressions given by Blakeslee & Tonry (1995). Because the data go well beyond the turnover in the globular cluster luminosity function, the median correction for the full sample of galaxies was only 0.024 mag, with a range from 0.006 to 0.08 mag. As in ACSVCS-V, we assign a 25% uncertainty to this correction.

For each galaxy, we then have a set of corrected $\overline{z}_{850}$ measurements over different radial ranges. We measure the

---

[10] http://www.stsci.edu/hst/acs/analysis/zeropoints.

[11] http://idlastro.gsfc.nasa.gov/.

Figure 1. SBF $\overline{z}_{850}$ magnitude as a function of $(g_{475}-z_{850})$ color for individual annuli (diamonds) within the ACSFCS galaxies. The curve is a third-order polynomial fit to the full set of annuli after median-smoothing; it is used to reject annuli that are 3σ outliers with respect to the shifted relation defined by each galaxy's set of annuli. The small points show the rejected annuli. The large solid diamonds highlight the annuli of NGC 1399 (FCC213), the galaxy with the largest number of usable annuli.

Figure 2. Mean SBF $\overline{z}_{850}$ magnitude vs. $(g_{475}-z_{850})$ color for the 43 ACSFCS galaxies. The top panel shows the linear (green dashed line), quadratic (solid black curve), and cubic (blue dashed curve) polynomial fits to these averaged data, as well as the cubic polynomial fit to the annuli from Figure 1 (red dot-dashed curve). The quadratic and cubic fits to these data have very similar rms scatters of 0.092 and 0.091 mag, respectively. The lower panel shows the residuals with respect to the quadratic fit; the galaxies are labeled by their FCC numbers.

galaxy colors in the same annuli, with the same masks applied, and estimate the errors based on detector and shot noise, sky uncertainties in each bandpass (ACSFCS-I), and an assumed 1% flat-fielding positional error in the photometry (e.g., Sirianni et al. 2005). Figure 1 shows the measurements for all annuli. As in ACSVCS-V, we find that $\overline{z}_{850}$ becomes fainter as $(g_{475}-z_{850})$ gets redder, and the relation steepens at the red end. We can use this relation to reject discordant annuli before averaging. We did this by first median filtering the relation using steps of 0.04 mag in $(g_{475}-z_{850})$, then fitting a cubic (third-order) polynomial to the median-filtered relation. The curve in Figure 1 shows the result.

We assume that the annuli in each galaxy should follow the same general relation, but with a shift depending on the galaxy distance, and we used this to reject any annuli more than 3σ discrepant from the shifted relation for each galaxy. This process eliminates 15% of the galaxy annuli, or an average of about one annulus per galaxy. The rejected annuli, shown as small dots in Figure 1, are usually the innermost or outermost ones. They are non-Gaussian outliers that may be affected by poor model residuals or imperfect masking of chip defects, real objects, or clumpy dust. A similar culling of annuli was conducted for the ACSVCS SBF analysis, and we have simply made it more automated. Following this, we average the measurements for the remaining annuli to obtain a single value of $\overline{z}_{850}$ and of $(g_{475}-z_{850})$ for each galaxy.

We could instead use the calibration effectively defined by the annuli to obtain a relative distance modulus for each annulus, then average these to obtain a single distance modulus for each galaxy. We have tested this approach, and the final results are insensitive to whether or not the averaging is done on the magnitudes and colors or on the distance moduli, as long as the same calibration relation is used. This is because the calibration is quite linear over the color range of any individual galaxy. For instance, in Figure 1 we have highlighted the annuli for NGC 1399, the galaxy with the most annuli remaining after the culling process. We chose to average SBF magnitudes and colors before applying the calibration in order to follow the same procedure as in ACSVCS-V, and to simplify the derivation of a

single, combined Virgo+Fornax SBF calibration, a primary goal of this investigation.

Figure 2 (top panel) plots the averaged $\overline{z}_{850}$ and $(g_{475}-z_{850})$ values for our 43 ACSFCS galaxies. The numbers appear in Table 1, along with the final distances derived in Section 4 and the common names for the galaxies. Magnitudes and colors are all corrected for Galactic extinction and reddening as described in Section 2. These data allow us to define a calibration for the variation in apparent SBF z_{850}-band magnitude on galaxy color based entirely on Fornax galaxies, analogous to that derived in ACSVCS-V for Virgo. Fitting a linear relation to the full sample of 43 Fornax galaxies, we find

$$\overline{z}_{850} = (29.517 \pm 0.016) + (1.50 \pm 0.15)\left[(g_{475}-z_{850})-1.3\right],$$
(2)

where the errors are determined from bootstrap resampling (e.g., Press et al. 1992), and the rms scatter in the fit is 0.10 mag. This relation is plotted in Figure 2. It is interesting to compare Equation (2) with the corresponding linear fit for Virgo from Equation (14) of ACSVCS-V. The slopes are consistent within the combined errors, and the zero points differ by 0.43 ± 0.03 mag. This is a measure of the relative distance modulus between Fornax and Virgo, to the extent that a linear fit provides an accurate description of the $\overline{z}_{850}$–$(g_{475}-z_{850})$ relation. However, ACSVCS-V concluded that the linear fit was inadequate. Similarly, we find that the relation for Fornax exhibits obvious curvature. The slope depends on the color range of the galaxies fitted, and if we omit the single galaxy at $(g_{475}-z_{850}) < 1$, the slope increases to 1.60.

Table 1
SBF Data for Fornax Galaxies

Galaxy (1)	$(g-z)$ (2)	$\overline{m}_z$ (3)	$(m-M)$ (4)	d (5)	B_T (6)	Name (7)
FCC19	1.066 ± 0.025	29.258 ± 0.036	31.534 ± 0.074	20.3 ± 0.7	15.2	ESO301-08
FCC21	1.368 ± 0.007	29.676 ± 0.020	31.606 ± 0.065	21.0 ± 0.6	9.4	NGC1316
FCC26[a]	0.830 ± 0.025	28.974 ± 0.055	31.489 ± 0.139	19.9 ± 1.3	15.0	ESO357-25
FCC43	1.154 ± 0.007	29.283 ± 0.039	31.485 ± 0.073	19.8 ± 0.7	13.5	ESO358-01
FCC47	1.298 ± 0.013	29.271 ± 0.040	31.314 ± 0.075	18.3 ± 0.6	13.3	NGC1336
FCC55	1.248 ± 0.008	29.492 ± 0.051	31.598 ± 0.080	20.9 ± 0.8	13.9	ESO358-06
FCC63	1.373 ± 0.029	29.548 ± 0.019	31.470 ± 0.083	19.7 ± 0.8	12.7	NGC1339
FCC83	1.363 ± 0.017	29.482 ± 0.020	31.422 ± 0.071	19.2 ± 0.6	12.3	NGC1351
FCC90	1.013 ± 0.047	29.126 ± 0.144	31.445 ± 0.193	19.5 ± 1.7	15.0	. . .
FCC95	1.262 ± 0.013	29.385 ± 0.037	31.476 ± 0.073	19.7 ± 0.7	14.6	. . .
FCC100	1.105 ± 0.011	29.324 ± 0.048	31.568 ± 0.078	20.6 ± 0.7	15.5	. . .
FCC106	1.186 ± 0.017	29.320 ± 0.025	31.493 ± 0.068	19.9 ± 0.6	15.1	. . .
FCC119	1.182 ± 0.018	29.363 ± 0.077	31.539 ± 0.100	20.3 ± 0.9	15.0	. . .
FCC136	1.218 ± 0.020	29.248 ± 0.038	31.388 ± 0.075	18.9 ± 0.7	14.8	. . .
FCC143	1.273 ± 0.035	29.350 ± 0.041	31.427 ± 0.086	19.3 ± 0.8	14.3	NGC1373
FCC147	1.376 ± 0.014	29.543 ± 0.023	31.458 ± 0.070	19.6 ± 0.6	11.9	NGC1374
FCC148	1.225 ± 0.009	29.367 ± 0.037	31.500 ± 0.072	19.9 ± 0.7	13.6	NGC1375
FCC152	1.125 ± 0.011	29.130 ± 0.021	31.357 ± 0.065	18.7 ± 0.6	14.1	ESO358-25
FCC153	1.262 ± 0.009	29.498 ± 0.034	31.588 ± 0.071	20.8 ± 0.7	13.0	ESO358-26
FCC167	1.394 ± 0.019	29.750 ± 0.021	31.632 ± 0.075	21.2 ± 0.7	11.3	NGC1380
FCC170	1.376 ± 0.019	29.790 ± 0.028	31.705 ± 0.076	21.9 ± 0.8	13.0	NGC1381
FCC177	1.257 ± 0.009	29.412 ± 0.019	31.509 ± 0.065	20.0 ± 0.6	13.2	NGC1380A
FCC182	1.302 ± 0.029	29.421 ± 0.044	31.458 ± 0.086	19.6 ± 0.8	14.9	. . .
FCC184	1.517 ± 0.011	29.857 ± 0.052	31.430 ± 0.087	19.3 ± 0.8	12.3	NGC1387
FCC190	1.352 ± 0.016	29.581 ± 0.029	31.540 ± 0.073	20.3 ± 0.7	13.5	NGC1382[b]
FCC193	1.369 ± 0.010	29.699 ± 0.033	31.627 ± 0.072	21.2 ± 0.7	12.8	NGC1389
FCC202	1.157 ± 0.049	29.312 ± 0.036	31.511 ± 0.083	20.1 ± 0.8	15.3	NGC1396
FCC203	1.169 ± 0.010	29.390 ± 0.055	31.579 ± 0.082	20.7 ± 0.8	15.5	ESO358-42
FCC204	1.233 ± 0.011	29.495 ± 0.043	31.619 ± 0.075	21.1 ± 0.7	14.9	ESO358-43
FCC213	1.500 ± 0.022	29.972 ± 0.020	31.596 ± 0.091	20.9 ± 0.9	10.6	NGC1399
FCC219	1.479 ± 0.013	29.842 ± 0.016	31.526 ± 0.072	20.2 ± 0.7	10.9	NGC1404
FCC249	1.295 ± 0.022	29.752 ± 0.045	31.799 ± 0.082	22.9 ± 0.9	13.6	NGC1419
FCC255	1.197 ± 0.013	29.340 ± 0.023	31.502 ± 0.067	20.0 ± 0.6	13.7	ESO358-50
FCC276	1.366 ± 0.007	29.524 ± 0.026	31.459 ± 0.068	19.6 ± 0.6	11.8	NGC1427
FCC277	1.313 ± 0.011	29.558 ± 0.046	31.579 ± 0.078	20.7 ± 0.7	13.8	NGC1428
FCC288	1.124 ± 0.009	29.453 ± 0.050	31.680 ± 0.079	21.7 ± 0.8	15.4	ESO358-56
FCC301	1.232 ± 0.013	29.348 ± 0.047	31.473 ± 0.078	19.7 ± 0.7	14.2	ESO358-59
FCC303	1.143 ± 0.017	29.261 ± 0.043	31.471 ± 0.076	19.7 ± 0.7	15.5	. . .
FCC310	1.314 ± 0.007	29.479 ± 0.020	31.499 ± 0.065	19.9 ± 0.6	13.5	NGC1460
FCC324	1.156 ± 0.010	29.314 ± 0.044	31.514 ± 0.076	20.1 ± 0.7	15.3	ESO358-66
FCC335	1.131 ± 0.013	29.220 ± 0.029	31.442 ± 0.068	19.4 ± 0.6	14.2	ESO359-02
NGC1340	1.314 ± 0.007	29.583 ± 0.028	31.603 ± 0.068	20.9 ± 0.7	11.3	NGC1344[c]
IC2006	1.422 ± 0.016	29.702 ± 0.049	31.525 ± 0.086	20.2 ± 0.8	12.2	ESO359-07

Notes.

[a] The distance calibration is less well constrained at these blue colors.

[b] Also known as NGC1380B.

[c] Due to an apparent error in the catalogue, this galaxy has two NGC numbers.

Columns list: (1) FCC designation (Ferguson 1989); (2) mean $(g_{475}-z_{850})$ color of the analyzed region; (3) mean SBF magnitude $\overline{m}_z$; (4) distance modulus derived from Equation (6); (5) distance in Mpc; (6) total B magnitude from the FCC or NED; (7) common galaxy name. The B_T column facilitates comparison to tables in other papers of this series where the galaxies are ordered by this quantity.

We also show second- and third-order polynomial fits to the $\overline{z}_{850}-(g_{475}-z_{850})$ relation in Figure 2 and compare the fitted relation for the annuli from Figure 1. For this sample of SBF measurements, a quadratic fit provides an adequate description to the curvature in the relation, and higher-order polynomials do not significantly decrease the rms scatter. The relation is poorly constrained for $(g_{475}-z_{850}) < 1$, where there is only a single galaxy. The lower panel of Figure 2 shows the residuals with respect to the quadratic relation. The rms scatter is 0.092 mag, and the largest outlier, at 0.26 mag or (2.8 σ), is FCC249. The next largest outlier is FCC47 at just under 2.5 σ.

The tight relation between the Fornax $\overline{z}_{850}$ magnitudes and $(g_{475}-z_{850})$ colors allows us to obtain, for the first time, a reasonably well-constrained estimate of the intrinsic, or "cosmic," scatter in this relation. We can estimate the expected depth of Fornax using the rms positional scatter of the sample galaxies on the sky. We find a scatter of 1°462 in right ascension and 1°335 in declination. We estimate the rms depth in magnitudes as

$$\sigma_{\rm est} = \sqrt{\frac{1}{2}(\sigma_{\rm R.A.}^2 + \sigma_{\rm decl.}^2)} \times \frac{\pi}{180} \times \frac{5}{\ln 10} \text{ mag}, \quad (3)$$

where $\sigma_{\text{R.A.}}$ and $\sigma_{\text{decl.}}$ are the rms positional scatters in degrees of arc. We find $\sigma_{\text{est}} = 0.053$ mag for Fornax. The mean observational error in distance for our sample due to the combined errors in $\overline{z}_{850}$ and $(g_{475}-z_{850})$ is 0.047 mag (the median is 0.042 mag). We can therefore estimate the cosmic scatter in the $\overline{z}_{850}-(g_{475}-z_{850})$ relation as

$$\sigma_{\text{cos}} \approx \sqrt{\sigma_o^2 - \sigma_{\text{est}}^2 - \sigma_{\text{err}}^2} \qquad (4)$$
$$\approx 0.060 \text{ mag},$$

where $\sigma_o = 0.092$ mag is the observed scatter in the relation and σ_{err} is the typical measurement error. Thus, unlike in Virgo, the estimated depth of the cluster is less than the intrinsic scatter in the method. Of course, the value of σ_{cos} is still somewhat degenerate with assumptions about the cluster depth. We examine these issues through a more careful χ^2 analysis in the following section, and discuss specific limits on cosmic scatter and cluster depth in Section 5.3.

4. COMBINED SBF CALIBRATION AND THE FORNAX–VIRGO RELATIVE DISTANCE

We now combine our ACS Fornax and Virgo survey measurements to obtain an improved calibration. We first look at the color distributions of the galaxies in the two samples. Figure 3 displays the $(g_{475}-z_{850})$ histogram for the total sample of 128 galaxies in Fornax and Virgo (omitting the more distant W' galaxies) with SBF measurements from the present work and from ACSVCS-XIII, respectively. The overall median color is 1.27 mag and the mean is $\langle g_{475}-z_{850}\rangle = 1.26 \pm 0.01$, which is the same as for the Fornax and Virgo samples individually (Figure 3 inset). The color distribution is somewhat broader for Virgo, which has an rms scatter $\sigma_{g-z} = 0.16 \pm 0.01$ mag, compared to $\sigma_{g-z} = 0.13 \pm 0.02$ mag for Fornax. This is partly because there are more massive red ellipticals in Virgo, but also the Virgo sample is not complete and goes $\sim$1 mag deeper in terms of absolute B magnitude than the Fornax sample; it thus includes lower-mass, bluer galaxies. The color distribution is asymmetric with a tail to bluer colors. Omitting galaxies with $(g_{475}-z_{850}) < 1.02$, the mean and dispersion are respectively 1.29 and 0.13 for Virgo, and 1.27 and 0.11 for Fornax. Thus, the two samples have very similar mean colors, but the dispersion is slightly larger for Virgo.

4.1. The Combined Calibration

Given that the two samples are fairly similar, combining them and fitting for a single SBF–color relation and relative offset in distance is a reasonable approach. To this end, we minimize the value of χ^2 calculated as

$$\chi^2 = \sum_i^{N_V} \frac{\left[p_n(x_i) - \overline{z}_{850,i}\right]^2}{\sigma_{\text{err},i}^2 + \sigma_{\text{cos}}^2 + \sigma_{\text{est,Vir}}^2} + \sum_j^{N_F} \frac{\left[p_n(x_j) + \Delta - \overline{z}_{850,j}\right]^2}{\sigma_{\text{err},j}^2 + \sigma_{\text{cos}}^2 + \sigma_{\text{est,For}}^2},$$
$$(5)$$

where the two sums are over the N_V and N_F galaxies in Virgo and Fornax, respectively, p_n is a polynomial of order n, $x_i = (g_{475}-z_{850})_i - 1.3$, $\Delta = \Delta(m-M)_{\text{FV}}$ is the relative distance modulus between Fornax and Virgo, $\sigma_{\text{err},i}$ is the total observational error for each galaxy measured perpendicular to the polynomial (based on error estimates from Section 3), σ_{cos} is a fixed value for the cosmic scatter in the calibration, $\sigma_{\text{est,Vir}}$ is the rms depth in magnitudes of Virgo, and $\sigma_{\text{est,For}}$ is the rms depth in magnitudes of Fornax. In practice, we vary Δ over a
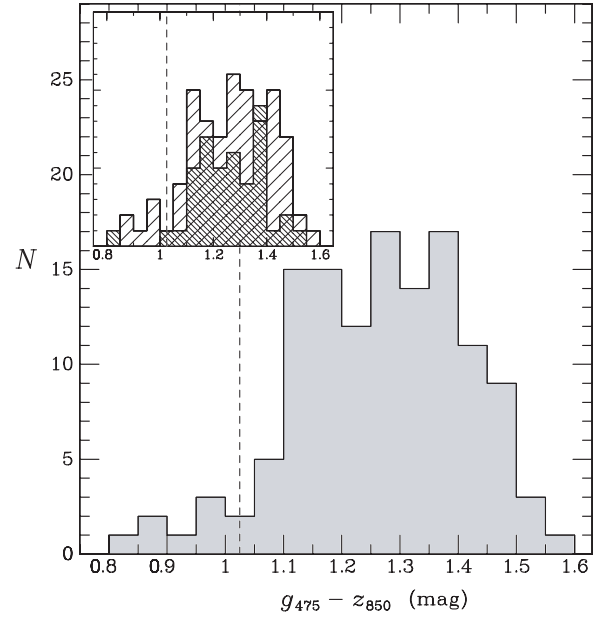
Figure 3. Galaxy $(g_{475}-z_{850})$ color histogram for the combined sample of 128 Fornax and Virgo galaxies with SBF measurements. The dashed line near $(g_{475}-z_{850}) = 1.02$ marks where the scatter in the SBF–color relation increases for bluer galaxies. Overall, the mean color is $(g_{475}-z_{850}) = 1.26\pm0.01$ and the rms dispersion is 0.15 mag; for the subsample omitting the blue tail, the mean and dispersion are 1.28 ± 0.01 and 0.12 mag, respectively. The inset shows the Virgo (broad hatching) and Fornax (narrow hatching) histograms plotted separately. The vertical ticks in the inset mark the same intervals as for the larger plot.

range of values and refit the polynomial calibration at each value. We omit the five Virgo W' galaxies from the χ^2 sum, as these are located 6.5 Mpc beyond the Virgo core (ACSVCS-XIII).

From Equation (3), we estimated the rms depth of Fornax to be $\sigma_{\text{est,For}} = 0.053$ mag. Doing the same calculation for the Virgo sample gives $\sigma_{\text{est,Vir}} = 0.085$ mag. Thus, the expected depth scatter is about 40% less for Fornax, which is a prime motivation for its frequent use as a distance method calibrator. These numbers agree well with the rms depths of 0.055 mag and 0.082 mag adopted by Tonry et al. (2000) for Fornax and Virgo, respectively, based on smaller samples of galaxies. (The significantly larger value quoted for the expected rms depth of Virgo in ACSVCS-V and ACSVCS-XIII resulted from the omission of the factor of $\frac{1}{\sqrt{2}}$ in the evaluation of Equation (3).)

In practice, we have found from the χ^2 analysis that the assumption of a single fixed value for σ_{cos} is a good approximation only at colors $(g_{475}-z_{850}) \gtrsim 1.02$ mag, similar to the conclusions of ACSVCS-V. Minimizing χ^2 for the subsample of 119 galaxies (77 in Virgo, 42 in Fornax) with $(g_{475}-z_{850}) > 1.02$, we find that a second-order polynomial gives the best value of the reduced χ^2, and that this value reaches $\chi_N^2 = 1.0$ for the best-fit model when $\sigma_{\text{cos}} = 0.064$ mag. This value of σ_{cos} is more dependent on the Fornax galaxies because σ_{cos} is larger than the magnitude depth of Fornax but smaller than the depth of Virgo.

There is one galaxy in Fornax (FCC249) that is a nonstatistical, 3.5σ outlier from the best-fit combined calibration. Like the W' galaxies in Virgo, it may simply be more distant than the rest of the cluster. The next largest outlier in Fornax is 2.6 σ. If we omit FCC249 and refit the second-order calibration for galaxies with $(g_{475}-z_{850}) > 1.02$, we obtain $\chi_N^2 = 1.0$ for the best-fit model when $\sigma_{\text{cos}} = 0.059$ mag, very similar to the result
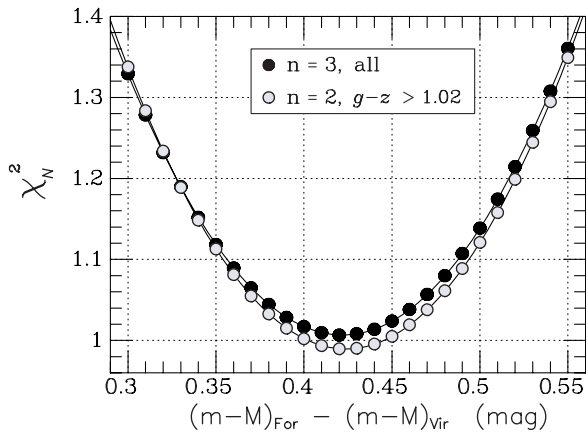
Figure 4. Reduced χ^2 as a function of the relative Fornax–Virgo distance modulus $\Delta(m-M)_{\rm FV}$ for a second-order polynomial fit to the combined $\overline{z}_{850}-(g_{475}-z_{850})$ relation for 118 Fornax and Virgo galaxies with $(g_{475}-z_{850}) > 1.02$ (gray circles) and for a third-order polynomial fit to 127 Virgo and Fornax galaxies over the full color range (filled black circles). The number of free parameters is equal to the order of the polynomial plus one (the relative distance modulus). Thus, the $n = 2, 3$ order fits have 115 and 123 degrees of freedom, respectively. In both cases, we use allowances for cluster depth as described in the text, and a "cosmic," or internal, scatter in the method of 0.06 mag (adjusted to give $\chi^2_N \approx 1.0$) for the galaxies with $(g_{475}-z_{850}) > 1.02$. The eight bluer galaxies require a larger internal scatter of ~ 0.13 mag. The value of χ^2 is computed here at increments of 0.01 mag, and the curves show that a quadratic provides excellent fits, with minima at $\Delta(m-M)_{\rm FV} = 0.424 \pm 0.020$ ($n = 2$) and $\Delta(m-M)_{\rm FV} = 0.422 \pm 0.019$ ($n = 3$).

for our more approximate calculation in the preceding section based on Fornax alone. In ACSVCS-V, a value of $\sigma_{\rm cos} = 0.05$ was assumed, but no constraints were possible, given that the assumed depth of Virgo in that paper was more than twice as large. Formally, the value of the total χ^2 changes by 1.0 when $\sigma_{\rm cos}$ is changed in our analysis by only 0.001 mag. This reflects the precision of the ACS SBF measurements and the small depth of Fornax. However, the depth of Fornax is uncertain by at least 15%, based on bootstrap resampling of the galaxy positions used in the calculation of Equation (3) and could be larger if the cluster were elongated along the line of sight. If we therefore assume a depth uncertainty of 20%, then we estimate values of the cosmic scatter and its 1σ uncertainty of $\sigma_{\rm cos} \approx 0.06 \pm 0.01$ mag, which we henceforth adopt for galaxies with $(g_{475}-z_{850}) > 1.02$ mag.

Figure 4 shows the values of the reduced χ^2 as a function of the relative Fornax–Virgo distance modulus $\Delta(m-M)_{\rm FV}$ (represented by Δ in Equation (5)). The gray circles show the χ^2_N values for the quadratic polynomial, using galaxies with $(g_{475}-z_{850}) > 1.02$. The best-fit relative distance modulus is $\Delta(m-M)_{\rm FV} = 0.424 \pm 0.020$ mag. The identical error bar is obtained from the χ^2 analysis as from bootstrap resampling. The solid black circles in the figure show χ^2_N values for a cubic polynomial fit to the full range of galaxy colors. The cubic polynomial gives a small but significant improvement in this case; higher-order polynomials are not warranted. However, in order to obtain $\chi^2_N \approx 1.0$, as is Figure 4, it is necessary to use a larger intrinsic scatter of $\sigma_{\rm cos,blue} = 0.13$ mag for the blue tail of galaxies at $(g_{475}-z_{850}) < 1.02$. This is mostly driven by the scatter for the blue Virgo galaxies. The best-fit relative distance modulus in this case is $\Delta(m-M)_{\rm FV} = 0.422 \pm 0.019$, virtually unchanged. We note that if we include the galaxy FCC249 and repeat the analysis, the best-fit relative distance modulus increases by 0.005 mag.

The combined cubic polynomial calibration is presented in Figure 5. The top panel shows the Virgo and Fornax galaxies
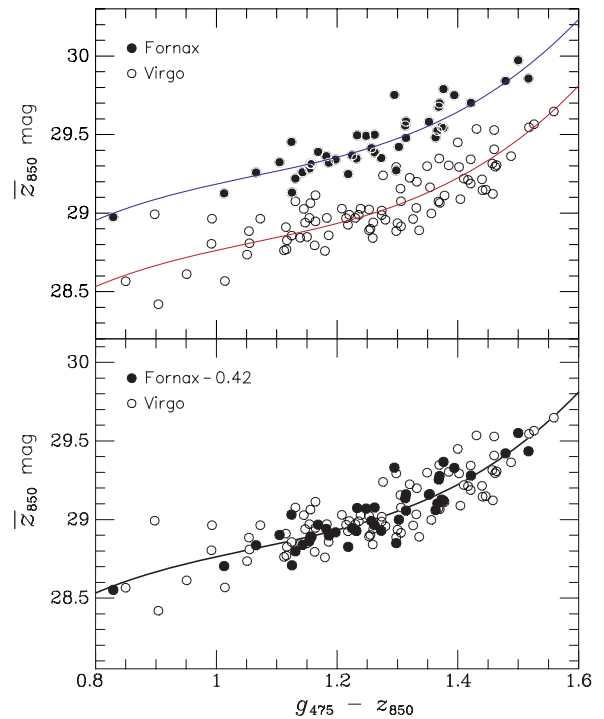
Figure 5. SBF $\overline{z}_{850}$ magnitude vs. $(g_{475}-z_{850})$ color for our ACS Virgo and Fornax cluster survey galaxies. The top panel shows the cubic polynomial fit to the full sample of galaxies (omitting the W' galaxies, not plotted). The relative Fornax–Virgo distance modulus $\Delta(m-M)_{\rm FV}$ is a free parameter, and the fit is done by minimizing χ^2, including errors in both coordinates. The lower panel shows the two samples shifted together by subtracting the best-fit value $\Delta(m-M)_{\rm FV} = 0.42 \pm 0.02$ mag from the Fornax galaxy distance moduli.

(A color version of this figure is available in the online journal.)

prior to shifting; the bottom panel shows the clusters shifted together by the best-fit $\Delta(m-M)_{\rm FV}$. Assuming a distance modulus of 31.09 mag for the Virgo cluster as in ACSVCS-XIII, we determine a final calibration for the absolute z_{850} SBF magnitude of

$$\overline{M}_z = -2.04 + 1.41x + 2.60x^2 + 3.72x^3, \qquad (6)$$

where $x \equiv (g_{475}-z_{850}) - 1.3$, and Equation (6) is valid for $0.8 \lesssim (g_{475}-z_{850}) \lesssim 1.6$. The smooth, continuous variation of $\overline{M}_z$ with $(g_{475}-z_{850})$ indicates there is no dwarf–giant dichotomy with respect to stellar population properties, apart from an increased scatter for the bluest galaxies. The precise form of the calibration is uncertain for $(g_{475}-z_{850}) \lesssim 1$ mag because of the larger scatter and low number of points. The statistical error on the $\overline{M}_z$ zero point in Equation (6) is 0.01 mag, but the systematic uncertainty due to the distance of Virgo is ~ 0.15 mag, based on the zero-point uncertainty of the Cepheid distance scale (Freedman et al. 2001; Macri et al. 2006) and the tie between the Cepheid and early-type galaxy (SBF) distance scales (Tonry et al. 2001, hereafter Ton01).

The resulting Fornax distance modulus is $(m - M)_{\rm For} = 31.51 \pm 0.02 \pm 0.15$ mag, corresponding to a distance $d_F = 20.0 \pm 0.2 \pm 1.4$ Mpc. Based on their positions in the sky, the three-dimensional distance between the center of Virgo and the center of Fornax is then 33.4 Mpc. Table 1 lists our final galaxy distances calibrated using Equation (6), and Table 2 presents the data and homogeneously calibrated distances for the ACSVCS galaxies, plus NGC 4697, the dominant elliptical member of a group in the Virgo Southern Extension (e.g.,

Table 2
SBF Data for Virgo Galaxies

Galaxy (1)	$(g-z)$ (2)	$\overline{m}_z$ (3)	$(m-M)$ (4)	d (5)	B_T (6)	Name (7)
VCC9	1.054 ± 0.014	28.885 ± 0.066	31.170 ± 0.091	17.1 ± 0.7	13.9	IC3019
VCC21[a]	0.898 ± 0.015	28.993 ± 0.040	31.421 ± 0.130	19.2 ± 1.1	14.8	IC3025
VCC33	1.014 ± 0.014	28.568 ± 0.051	30.886 ± 0.133	15.0 ± 0.9	14.7	IC3032
VCC140	1.125 ± 0.014	28.857 ± 0.040	31.084 ± 0.074	16.5 ± 0.6	14.3	IC3065
VCC200	1.164 ± 0.014	29.114 ± 0.050	31.307 ± 0.080	18.3 ± 0.7	14.7	. . .
VCC230	1.156 ± 0.014	29.063 ± 0.091	31.263 ± 0.110	17.9 ± 0.9	15.2	IC3101
VCC355	1.404 ± 0.014	29.089 ± 0.024	30.950 ± 0.072	15.5 ± 0.5	12.4	NGC4262
VCC369	1.440 ± 0.014	29.215 ± 0.022	30.996 ± 0.073	15.8 ± 0.5	11.8	NGC4267
VCC437	1.208 ± 0.014	29.029 ± 0.049	31.180 ± 0.080	17.2 ± 0.6	14.5	UGC7399A
VCC538[b]	1.110 ± 0.014	29.572 ± 0.064	31.812 ± 0.089	23.0 ± 0.9	15.4	NGC4309A
VCC543	1.163 ± 0.014	28.795 ± 0.045	30.989 ± 0.077	15.8 ± 0.6	14.4	UGC7436
VCC571[b]	1.063 ± 0.014	29.607 ± 0.078	31.885 ± 0.100	23.8 ± 1.1	14.7	. . .
VCC575[b]	1.272 ± 0.014	29.639 ± 0.041	31.716 ± 0.076	22.0 ± 0.8	14.1	NGC4318
VCC698	1.298 ± 0.014	29.294 ± 0.032	31.337 ± 0.072	18.5 ± 0.6	13.6	NGC4352
VCC731[b]	1.489 ± 0.014	30.161 ± 0.015	31.816 ± 0.074	23.1 ± 0.8	10.5	NGC4365
VCC751	1.253 ± 0.014	28.891 ± 0.046	30.992 ± 0.078	15.8 ± 0.6	15.3	IC3292
VCC759	1.460 ± 0.014	29.407 ± 0.018	31.139 ± 0.073	16.9 ± 0.6	11.8	NGC4371
VCC763	1.431 ± 0.014	29.535 ± 0.013	31.337 ± 0.070	18.5 ± 0.6	10.3	NGC4374, M84
VCC778	1.320 ± 0.014	29.225 ± 0.030	31.236 ± 0.071	17.7 ± 0.6	12.7	NGC4377
VCC784	1.368 ± 0.014	29.073 ± 0.024	31.004 ± 0.070	15.9 ± 0.5	12.7	NGC4379
VCC798	1.349 ± 0.014	29.298 ± 0.013	31.262 ± 0.067	17.9 ± 0.5	10.1	NGC4382, M85
VCC828	1.369 ± 0.014	29.347 ± 0.031	31.276 ± 0.073	18.0 ± 0.6	12.8	NGC4387
VCC856	1.164 ± 0.014	28.947 ± 0.044	31.140 ± 0.076	16.9 ± 0.6	14.2	IC3328
VCC881[c]	1.460 ± 0.014	29.529 ± 0.013	31.261 ± 0.072	17.9 ± 0.6	10.1	NGC4406, M86
VCC944	1.378 ± 0.014	29.112 ± 0.021	31.024 ± 0.070	16.0 ± 0.5	12.1	NGC4417
VCC1025[b]	1.380 ± 0.015	29.850 ± 0.030	31.759 ± 0.074	22.5 ± 0.8	13.1	NGC4434
VCC1030	1.306 ± 0.014	29.076 ± 0.020	31.107 ± 0.067	16.7 ± 0.5	11.8	NGC4435
VCC1049	1.051 ± 0.014	28.736 ± 0.045	31.023 ± 0.077	16.0 ± 0.6	14.2	UGC7580
VCC1062	1.441 ± 0.014	29.146 ± 0.018	30.925 ± 0.072	15.3 ± 0.5	11.4	NGC4442
VCC1075	1.150 ± 0.014	28.848 ± 0.076	31.054 ± 0.098	16.2 ± 0.7	15.1	IC3383
VCC1087	1.236 ± 0.014	28.989 ± 0.040	31.110 ± 0.075	16.7 ± 0.6	14.3	IC3381
VCC1146	1.274 ± 0.014	28.988 ± 0.028	31.063 ± 0.070	16.3 ± 0.5	12.9	NGC4458
VCC1154	1.462 ± 0.014	29.295 ± 0.020	31.022 ± 0.073	16.0 ± 0.5	11.4	NGC4459
VCC1178	1.370 ± 0.014	29.066 ± 0.031	30.993 ± 0.073	15.8 ± 0.5	13.4	NGC4464
VCC1185	1.239 ± 0.014	29.028 ± 0.089	31.145 ± 0.109	16.9 ± 0.9	15.7	. . .
VCC1226	1.518 ± 0.014	29.546 ± 0.011	31.116 ± 0.075	16.7 ± 0.6	9.3	NGC4472, M49
VCC1231	1.446 ± 0.014	29.149 ± 0.017	30.916 ± 0.072	15.2 ± 0.5	11.1	NGC4473
VCC1242	1.306 ± 0.014	28.915 ± 0.048	30.946 ± 0.080	15.5 ± 0.6	12.6	NGC4474
VCC1250	1.145 ± 0.014	29.027 ± 0.049	31.237 ± 0.079	17.7 ± 0.6	12.9	NGC4476
VCC1261	1.131 ± 0.014	29.076 ± 0.035	31.298 ± 0.071	18.2 ± 0.6	13.6	NGC4482
VCC1279	1.402 ± 0.014	29.294 ± 0.023	31.159 ± 0.071	17.1 ± 0.6	12.2	NGC4478
VCC1283	1.385 ± 0.014	29.304 ± 0.030	31.203 ± 0.073	17.4 ± 0.6	13.4	NGC4479
VCC1297	1.457 ± 0.014	29.315 ± 0.045	31.055 ± 0.084	16.3 ± 0.6	14.3	NGC4486B
VCC1303	1.354 ± 0.014	29.164 ± 0.027	31.120 ± 0.071	16.7 ± 0.5	13.1	NGC4483
VCC1316	1.526 ± 0.014	29.566 ± 0.012	31.111 ± 0.076	16.7 ± 0.6	9.6	NGC4486, M87
VCC1321	1.259 ± 0.014	28.841 ± 0.028	30.935 ± 0.069	15.4 ± 0.5	12.8	NGC4489
VCC1327	1.400 ± 0.014	29.450 ± 0.030	31.319 ± 0.074	18.4 ± 0.6	13.3	NGC4486A
VCC1355	1.115 ± 0.014	28.910 ± 0.063	31.145 ± 0.088	16.9 ± 0.7	14.3	IC3442
VCC1407	1.220 ± 0.014	28.990 ± 0.030	31.128 ± 0.070	16.8 ± 0.5	15.5	IC3461
VCC1422	1.180 ± 0.014	28.759 ± 0.039	30.937 ± 0.074	15.4 ± 0.5	13.6	IC3468
VCC1431	1.280 ± 0.014	28.958 ± 0.042	31.025 ± 0.076	16.0 ± 0.6	14.5	IC3470
VCC1440	1.186 ± 0.014	28.858 ± 0.048	31.030 ± 0.079	16.1 ± 0.6	15.2	IC798
VCC1475	1.215 ± 0.014	28.968 ± 0.032	31.111 ± 0.070	16.7 ± 0.5	13.4	NGC4515
VCC1488[a]	0.850 ± 0.014	28.566 ± 0.053	31.053 ± 0.134	16.2 ± 1.0	14.8	IC3487
VCC1489[a]	0.993 ± 0.014	28.964 ± 0.097	31.299 ± 0.156	18.2 ± 1.3	15.9	IC3490
VCC1512	1.276 ± 0.014	29.240 ± 0.030	31.312 ± 0.070	18.3 ± 0.6	15.7	. . .
VCC1528	1.218 ± 0.014	28.926 ± 0.043	31.066 ± 0.076	16.3 ± 0.6	14.5	IC3501
VCC1537	1.300 ± 0.014	28.936 ± 0.029	30.976 ± 0.070	15.7 ± 0.5	12.7	NGC4528
VCC1539	1.147 ± 0.014	28.939 ± 0.102	31.147 ± 0.119	17.0 ± 0.9	15.7	. . .
VCC1545	1.253 ± 0.014	29.023 ± 0.050	31.124 ± 0.081	16.8 ± 0.6	15.0	IC3509
VCC1619	1.298 ± 0.014	28.886 ± 0.022	30.929 ± 0.068	15.3 ± 0.5	12.5	NGC4550
VCC1627[d]	1.326 ± 0.130	28.962 ± 0.049	30.963 ± 0.217	15.6 ± 1.6	15.2	. . .
VCC1630	1.417 ± 0.014	29.212 ± 0.028	31.045 ± 0.074	16.2 ± 0.5	12.9	NGC4551
VCC1632[c]	1.488 ± 0.014	29.363 ± 0.013	31.021 ± 0.073	16.0 ± 0.5	10.8	NGC4552, M89
VCC1661	1.255 ± 0.014	28.901 ± 0.156	31.000 ± 0.168	15.8 ± 1.2	16.0	. . .

Table 2
(Continued)

Galaxy (1)	$(g-z)$ (2)	$\overline{m}_z$ (3)	$(m-M)$ (4)	d (5)	B_T (6)	Name (7)
VCC1664	1.421 ± 0.014	29.188 ± 0.021	31.013 ± 0.071	15.9 ± 0.5	12.0	NGC4564
VCC1692	1.421 ± 0.014	29.343 ± 0.020	31.168 ± 0.071	17.1 ± 0.6	11.8	NGC4570
VCC1695	1.055 ± 0.014	28.809 ± 0.050	31.093 ± 0.080	16.5 ± 0.6	14.5	IC3586
VCC1720	1.410 ± 0.014	29.220 ± 0.020	31.068 ± 0.071	16.4 ± 0.5	12.3	NGC4578
VCC1743	1.073 ± 0.014	28.964 ± 0.071	31.234 ± 0.094	17.6 ± 0.8	15.5	IC3602
VCC1779[a]	0.904 ± 0.014	28.420 ± 0.055	30.841 ± 0.135	14.7 ± 0.9	14.8	IC3612
VCC1826	1.117 ± 0.014	28.826 ± 0.060	31.060 ± 0.086	16.3 ± 0.6	15.7	IC3633
VCC1828	1.183 ± 0.014	28.970 ± 0.059	31.145 ± 0.086	16.9 ± 0.7	15.3	IC3635
VCC1833	1.139 ± 0.014	28.844 ± 0.041	31.059 ± 0.074	16.3 ± 0.6	14.5	. . .
VCC1861	1.260 ± 0.014	28.941 ± 0.045	31.034 ± 0.078	16.1 ± 0.6	14.4	IC3652
VCC1871	1.356 ± 0.014	28.998 ± 0.039	30.950 ± 0.076	15.5 ± 0.5	13.9	IC3653
VCC1883	1.274 ± 0.014	29.017 ± 0.023	31.092 ± 0.068	16.5 ± 0.5	12.6	NGC4612
VCC1886[a]	0.951 ± 0.014	28.612 ± 0.137	30.985 ± 0.184	15.7 ± 1.3	15.5	. . .
VCC1895	1.116 ± 0.014	28.770 ± 0.030	31.005 ± 0.069	15.9 ± 0.5	14.9	UGC7854
VCC1903	1.458 ± 0.014	29.122 ± 0.014	30.859 ± 0.072	14.9 ± 0.5	10.8	NGC4621, M59
VCC1910	1.331 ± 0.014	29.033 ± 0.034	31.027 ± 0.073	16.0 ± 0.5	14.2	IC809
VCC1913	1.332 ± 0.014	29.199 ± 0.028	31.191 ± 0.071	17.3 ± 0.6	13.2	NGC4623
VCC1938	1.305 ± 0.014	29.156 ± 0.024	31.189 ± 0.069	17.3 ± 0.5	12.1	NGC4638
VCC1948[a]	0.992 ± 0.014	28.804 ± 0.099	31.140 ± 0.158	16.9 ± 1.2	15.1	. . .
VCC1978	1.559 ± 0.014	29.647 ± 0.012	31.082 ± 0.079	16.5 ± 0.6	9.8	NGC4649, M60
VCC1993	1.230 ± 0.014	28.970 ± 0.030	31.097 ± 0.070	16.6 ± 0.5	15.3	. . .
VCC2000	1.336 ± 0.014	28.890 ± 0.024	30.876 ± 0.069	15.0 ± 0.5	11.9	NGC4660
VCC2019	1.154 ± 0.014	28.970 ± 0.045	31.172 ± 0.077	17.2 ± 0.6	14.6	IC3735
VCC2050	1.112 ± 0.014	28.762 ± 0.056	31.000 ± 0.084	15.8 ± 0.6	15.2	IC3779
VCC2092	1.464 ± 0.014	29.306 ± 0.018	31.028 ± 0.073	16.1 ± 0.5	11.5	NGC4754
NGC4697[e]	1.375 ± 0.008	28.573 ± 0.019	30.491 ± 0.065	12.5 ± 0.4	10.1	NGC4697

Notes.

[a] The distance calibration is less well constrained at these blue colors.

[b] Virgo W' group galaxy.

[c] There were typographical errors in the data for these galaxies in Table 1 of ACSVCS-XIII.

[d] This galaxy had incorrect distance moduli listed in Table 5 of ACSVCS-XIII.

[e] Member of a group in the Virgo Southern Extension; data described in Jordán et al. (2005).

Columns list: (1) VCC designation (Binggeli et al. 1985); (2) mean $(g_{475}-z_{850})$ color of the analyzed region from ACSVCS-XIII (Mei et al. 2007); (3) mean SBF magnitude $\overline{m}_z$ from ACSVCS-XIII; (4) distance modulus derived from Equation (6); (5) distance in Mpc; (6) total B magnitude from the VCC or NED; (7) common galaxy name. The B_T column facilitates comparison to tables in papers of the ACSVCS series where the galaxies are ordered by this quantity.

Tully 1982). In all, we tabulate new or recalibrated z_{850}-band SBF distances for 134 galaxies. The NGC 4697 observational details were identical to those of the ACSVCS galaxies and have been discussed by Jordán et al. (2005). The distance errors in Tables 1 and 2 are the quadrature sums of the measurement errors and the cosmic scatter $\sigma_{\rm cos}$, which is 0.06 mag for galaxies with $(g_{475}-z_{850}) > 1.02$, and approximated as twice this for bluer galaxies.

4.2. Possible Systematics

There are a few systematic differences between the Virgo and Fornax samples that could potentially affect the relative distance estimate. One is the mean $E(B-V)$ extinction correction: 0.028 mag for Virgo versus 0.013 mag for Fornax (Schlegel et al. 1998). The $E(B-V)$ corrections for the cD galaxies M87 and NGC 1399 are 0.022 and 0.013 mag, respectively. From Schlegel et al., the error on the extinction estimate is $\pm 16\%$ of the value itself. Because of the dependence of $\overline{M}_z$ on $(g_{475}-z_{850})$ color, and the total-to-selective extinction ratios for g_{475} and z_{850}, the error on $(m-M)$ using Equation (6) scales as $\delta(m-M) \approx -1.7\,\delta E(B-V) \approx \pm 0.27\,E(B-V)$. Because the mean extinctions toward Virgo and Fornax are both low, the quadrature sum of their distance errors from extinction is only ± 0.008 mag.

Another difference is in the date of the observations. The Fornax data were on average taken 1.5 yr after the Virgo data, and there is some evidence for small changes in the ACS/WFC photometric sensitivity during this period. Bohlin (2007) finds a decline in sensitivity of 0.002 ± 0.001 mag yr^{-1} for F475W and essentially no change for F850LP. Because of the color term in the $\overline{z}_{850}$ calibration and the 1.5 yr baseline, this translates to an error of -0.004 mag in $\Delta(m-M)_{\rm FV}$ (i.e., the value is underestimated). However, using a different technique, Riess (2004) earlier reported evidence for a sensitivity decline in F850LP similar to Bohlin's results at shorter wavelengths. If the degradation is independent of wavelength, then accounting for the effects on both $\overline{z}_{850}$ and color, the error in $\Delta(m-M)_{\rm FV}$ would be $\sim +0.004$ mag (the value is overestimated). Thus, we estimate the systematic uncertainty from this effect to be ± 0.004 mag. All of the data were taken before 2006 July when a significant change in sensitivity occurred because of a change in operating temperature (see Bohlin 2007).

One other potential difference is in the absolute zero point of the $\overline{z}_{850}$ versus $(g_{475}-z_{850})$ relations for Fornax and Virgo. Is the calibration truly universal, or could there be small cluster-to-cluster variations? Based on our analysis and the fit presented in Figure 5, the clusters appear to define a single relation. However, while there is an explicit correction for stellar population

based on $(g_{475}-z_{850})$, it is possible that systemic differences in the population parameters at a fixed color could cause small shifts in the zero point. This is because age and metallicity variations are not *exactly* degenerate in their effects on the relation between $\bar{z}_{850}$ and $(g_{475}-z_{850})$. For example, it could be that star formation began later in Fornax than in Virgo, so that the mean galaxy age is younger even at the same color. To assess the implications of this possibility, we selected subsets of the composite stellar population models described by Blakeslee et al. (2001b) and shown in ACSVCS-I. In one test, simulating a delay of several Gyr in the onset of galaxy formation, we selected only models where the old stellar component was at least 3 Gyr younger than the maximum stellar age in the ACSVCS-I models. This selection removed 56% of the models. We then refit the calibration. The scatter in the model $\bar{z}_{850}$ versus $(g_{475}-z_{850})$ relation went from 0.066 mag as reported in ACSVCS-I to 0.060 mag, our best empirical estimate for the intrinsic scatter in Fornax. The shift in zero point was 0.019 mag.

We tried other age selections that approximately preserved the overall color range but removed up to 79% of the composite models. The maximum zero-point shift from these tests was 0.026 mag, but more typically was $\lesssim 0.02$ mag. While an exhaustive treatment might involve analyzing the SBF relations in multiple clusters from detailed semianalytic simulations (which currently do not include SBF predictions), we conclude that 0.02 mag is a reasonable estimate of this systematic zero-point uncertainty. We add this in quadrature with the 0.02 mag statistical uncertainty and the small effects from extinction and ACS photometric sensitivity as described above. The total error on $\Delta(m-M)_{FV}$ is then ± 0.03 mag, and the Fornax distance is $d_F = 20.0 \pm 0.3 \pm 1.4$ Mpc.

4.3. Past Estimates of the Relative Distance

Before moving on to the discussion in the following section, we note that our result for the Fornax–Virgo relative distance modulus $\Delta(m-M)_{FV} = 0.42 \pm 0.03$ mag, which includes all systematic uncertainties, is well within the range of previous estimates. For instance, Ferrarese et al. (2000) tabulated values including 0.09 ± 0.27 mag from the globular cluster luminosity function (GCLF), 0.30 ± 0.10 mag from the planetary nebula luminosity function, and 0.40 ± 0.06 mag from ground-based I-band SBF. The difference of the weighted averages of the full samples of tabulated "good" SBF distances for Virgo and Fornax in Ton01 gives $\Delta(m-M)_{FV} = 0.36 \pm 0.05$ mag. The fundamental plane analysis by Kelson et al. (2000) implies $\Delta(m-M)_{FV} = 0.52 \pm 0.17$ mag. The one discrepant method among these appears to be the GCLF, suggesting an intrinsic difference in the mean luminosity of the globular clusters in these two systems (Blakeslee & Tonry 1996). This issue will be discussed in detail by another paper in our series.

The final *HST* Key Project Cepheid distances from Freedman et al. (2001) imply $\Delta(m-M)_{FV} = 0.47 \pm 0.21$ mag. The relatively large error bar is mainly due to the spread of 0.54 mag for the three Cepheid galaxies in Fornax. There is also good evidence that the Cepheid galaxies in both clusters avoid the core regions where early-type galaxies prevail. Despite their many virtues, Cepheids are therefore far from ideal for gauging the distances to galaxy clusters. Although our relative Fornax–Virgo distance is consistent with many previous studies, its precision is far greater. Because of the homogeneity of the ACSVCS and ACSFCS observations and SBF analyses, we believe that this level of precision reliably represents the accuracy of our relative distance measurement.
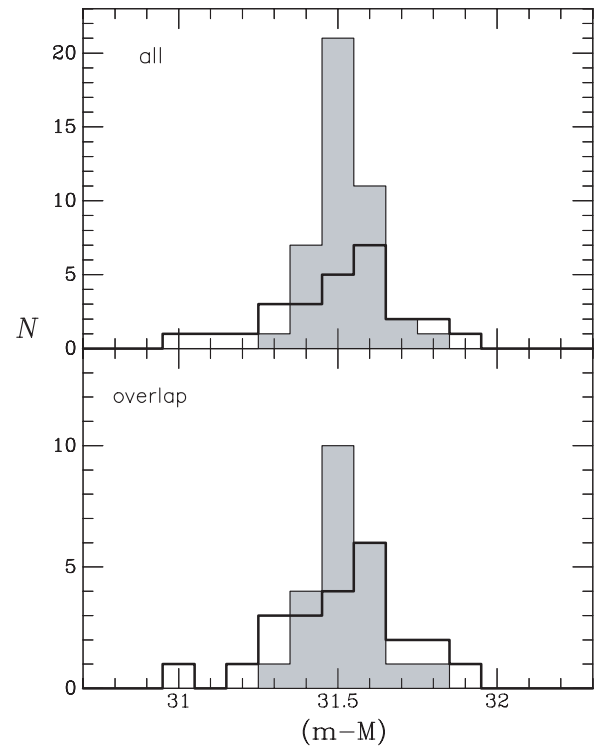
Figure 6. Fornax SBF distance moduli from our ACSFCS sample (gray histograms) and from the ground-based survey of Ton01 (thick-lined open histograms). The top panel shows the histograms for the full samples of 43 ACSFCS and 26 ground-based measurements; the lower panel shows histograms for the subsample of 23 galaxies in common between the two surveys (note different vertical ranges).

5. DISCUSSION

Our combined sample of SBF measurements for 134 early-type galaxies in the Virgo and Fornax clusters, Virgo W' group, and NGC 4697 in the Virgo Southern Extension constitutes the largest homogeneous set of SBF distances available. All were observed with the ACS/WFC for one orbit in the F850LP and F475W bandpasses. The ground-based I-band survey (Tonry et al. 1997; Ton01) of 300 galaxies was an ambitious, decade-long project, but heterogeneous in terms of seeing conditions, detectors, I-band filter characteristics, and telescopes. We now compare our results to those of some previous Fornax and Virgo SBF studies before going on to examine the questions of the structure of Fornax and a possible alternative calibration for our z_{850}-band SBF data.

5.1. Other Optical SBF Studies

There have been a number of studies of the SBF properties of Fornax cluster galaxies in both optical and near-IR passbands. The largest compilation of Fornax SBF data prior to our ACS survey was the subset of 26 ground-based I-band SBF measurements in Fornax from Ton01. The ACSFCS includes 23 of these galaxies. (Aside from NGC 1379, for which the *HST* observation failed, Ton01 observed NGC1366, which is outside the FCC survey area, and NGC1386, which is classified as Sa in the FCC.) Figure 6 compares the histograms of Fornax SBF distances from the two surveys. The top panel includes all Fornax galaxies in each survey; the lower panel includes the 23 galaxies in common.

As evident in Figure 6, the two surveys agree well in the mean, but our distance distribution is much tighter. The

median distance modulus for our full sample of 43 galaxies is 31.51 mag, and the observed rms dispersion is 0.092 mag. As discussed previously, the dispersion includes contributions from measurement error, intrinsic scatter, and Fornax depth. In comparison, the median of the 26 Ton01 distances is 31.52 mag and the rms dispersion is 0.21 mag. For the 23 galaxies in common, the median distance moduli again agree very closely and the rms dispersions are 0.11 mag and 0.20 mag for ACSFCS and Ton01, respectively. Allowing for the spread due to the estimated depth of 0.053 mag, our distances are more accurate by better than a factor of 2, and the measurement errors are smaller by a factor of 3 (but the intrinsic scatter of ~ 0.06 mag is common to both).

Comparing individual galaxies, we find that our distances agree with those of Ton01 to within the combined measurement error. The rms scatter of the differences is 0.24 mag, which is just slightly smaller than the quadrature sum of the average measurement errors. The reduced χ^2 value of the differences for these 23 galaxies is $\chi_N^2 = 0.93$. There are also 26 Virgo galaxies in common between ACSVCS and Ton01; the comparison of these was presented in ACSVCS-XIII. We now add NGC 4697 as well. Figure 7 compares the full set of 50 galaxies in common between our combined ACS sample and Ton01. These span a factor of nearly 2 in distance, and the reduced χ^2 of the differences is $\chi_N^2 = 1.01$. Fitting a linear relation with errors in both coordinates, we find

$$(m-M)_{\text{Ton01}} = (31.50 \pm 0.03) + (0.96 \pm 0.10)[(m-M)_{\text{ACS}} - 31.50]. \quad (7)$$

Thus, the surveys agree closely in the mean, and the slope is consistent with unity. The largest Fornax outlier is FCC177 (NGC 1380A), which we find to be at $(m-M) = 31.51$, while Ton01 find $(m-M) = 31.00 \pm 0.29$, a difference of less than 2σ. We note that ACS SBF measurements in the F814W bandpass (Cantiello et al. 2007a; Barber DeGraaff et al. 2007) also have high precision similar to our measurements and generally agree with Ton01, but occasionally reveal anomalous distances in the ground-based survey.

In addition to comparing the distances, since SBF studies require very accurate color data (or other spectral information suitable for calibration), we can compare our measured $(g_{475}-z_{850})$ to $(V-I)$ from Ton01. One complication is that galaxies have color gradients and the regions of the galaxies measured in the two surveys are generally different. The present survey analyzed regions of the galaxies at smaller radii, due to the smaller field of view, higher resolution, and finer pixel scale. To account for this effect in a similar comparison, Blakeslee et al. (2001a) derived an approximate transformation from the tabulated Ton01 $(V-I)$ values to the colors at a fixed radius of $10''$, which is within the range of radii measured here. As a first-order correction, we apply the same transformation, which we quote here to correct a typo in the original work: $(V-I)_{10''} = -0.046 + 1.05 (V-I)_{\text{Ton01}}$. The effect of this is to make the $(V-I)$ colors slightly redder.

Figure 8 presents the comparison of our $(g_{475}-z_{850})$ values with the transformed Ton01 colors. Fitting a linear relation with errors in both coordinates gives

$$(V-I) = (1.151 \pm 0.003 \pm 0.02) + (0.49 \pm 0.04)[(g_{475}-z_{850}) - 1.35], \quad (8)$$

where the second error bar on the zero point is the approximate systematic uncertainty in the tie of the ground-based data to
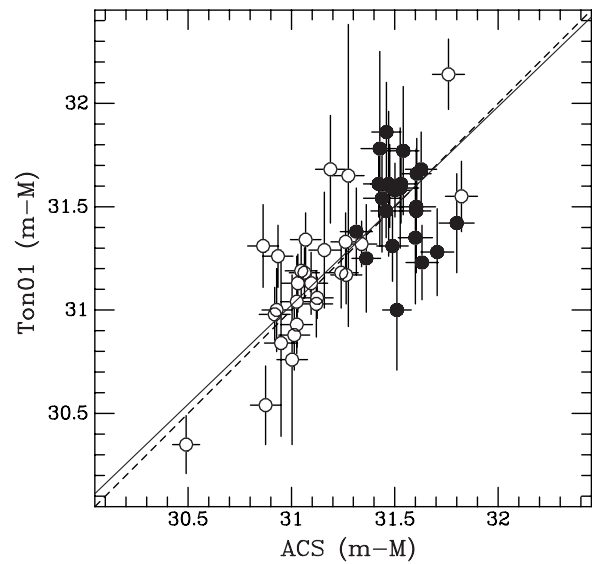
Figure 7. Comparison of the ground-based SBF distance moduli from Ton01 with our SBF distance moduli from the ACS Virgo (open circles) and Fornax (filled circles) cluster surveys. The solid line shows the best-fit linear relation using the errors in both coordinates, while the dashed line shows equality. The scatter in the vertical direction is larger than in the horizontal direction, but the overall agreement is good. The two "Virgo" galaxies with $(m-M) \approx 31.8$ are actually members of the background W' group. The galaxy with the lowest distance is NGC 4697.

Landolt (1992) standards and the absolute calibration of the Landolt $(V-I)$ colors to a Vega-based system. We note that Tonry et al. (1997) found a zero-point scatter in $(V-I)$ among different observing runs of about 0.02 mag. The run-to-run offsets were corrected by extensive intercomparisons, but the overall zero point for that survey likely had a similar uncertainty. The rms scatter in the fitted relation is 0.024 mag, which is larger than the combined observational error and suggests an additional scatter of ~ 0.015 mag due to stellar population and aperture effects. For comparison, we show the locus of solar-metallicity (Bruzual & Charlot 2003) models of varying ages. At a given $(g_{475}-z_{850})$, these are redder on average by about 0.02 mag in $(V-I)$, or bluer in $(g_{475}-z_{850})$ by 0.04 mag at a given $(V-I)$. This may result from uncorrected mean color gradients, but the agreement is reasonable given the likely uncertainties in observational and model color zero points.

There have been a few other optical SBF studies in Fornax, but the overlap with the present sample is much less. Blakeslee et al. (2001b) measured and calibrated V-band SBF magnitudes for the five brightest galaxies in the ACSFCS sample. Although the mean distance was lower by about 0.15 mag due to a different choice of zero-point calibration, the galaxies were consistent with being all at a common distance within the errors, the same as we find here. Jerjen (2003) and Dunn & Jerjen (2006) measured R-band SBF distances for a total of 18 dwarf FCC galaxies. However, only three of these galaxies overlap with our sample; the rest are fainter than our magnitude limit. For the three galaxies in common, the R-band SBF distances are larger by 0.21 ± 0.05 mag. However, this is probably due to small number statistics, as the overall mean distance modulus from Dunn & Jerjen is 31.50 mag, very similar to ours. The rms dispersion of their distance moduli is 0.21 mag, the same as in Ton01 and dominated by measurement errors. Finally, we note that Mieske et al. (2006) report I-band SBF measurements for 21 FCC dwarfs, mainly to evaluate the SBF scatter at blue colors, but all are quite faint and below our magnitude limit.
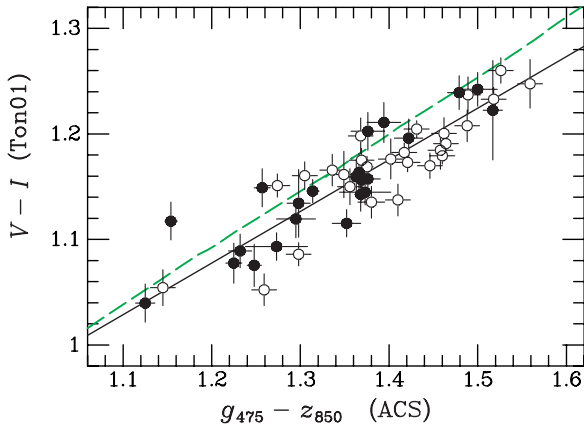
Figure 8. Comparison of the ground-based $(V-I)$ colors (Ton01) with our ACS $(g_{475}-z_{850})$ colors for the 23 Fornax (filled circles) and 26 Virgo (open circles) galaxies in common between these two surveys. The $(V-I)$ colors have been corrected according to the linear transformation derived by Blakeslee et al. (2001a). The solid line shows the best-fit relation using errors in both coordinates: $(V-I) \approx 1.15 + 0.5\,[(g-z)-1.35]$. For comparison, the dashed green line shows the locus of Bruzual & Charlot (2003) solar-metallicity models with ages in the range ~ 1.5 Gyr to 15 Gyr. The mean $(g_{475}-z_{850})$ color of this matched sample is significantly redder than the overall sample, since the ground-based survey targeted mainly giant galaxies.

(A color version of this figure is available in the online journal.)

5.2. Near-IR SBF in Fornax

In addition to the optical surveys, there have been two near-IR SBF studies including significant numbers of Fornax galaxies. In the first of these, Liu et al. (2002) measured ground-based K_s SBF magnitudes for 19 Fornax galaxies in $\sim 1''$ seeing with a 256^2 pixel IR array. There are 17 galaxies in common with our sample. The $\overline{K}_s$ distances show a large scatter when compared to ours, in excess of 0.4 mag, giving a very poor χ^2_N. This may reflect anomalous behavior of SBF in the K_s bandpass, with interesting stellar population implications. However, we believe it more likely reflects the difficulty in obtaining accurate ground-based K-band SBF measurements at a distance of 20 Mpc with a small detector, mediocre seeing, and a very bright sky background.

In another study, Jensen et al. (2003) measured SBF magnitudes for 19 Fornax and four Virgo galaxies (as part of a larger archival sample) in the NICMOS F160W bandpass (H_{160}). Their sample included the bulges of several spiral galaxies, and the main goal of this work was to calibrate the behavior $\overline{H}_{160}$ as a function of galaxy color. The ACSFCS and ACSVCS samples combined have 19 galaxies in common with Jensen et al. (2003), and we find it most interesting to present a direct comparison of the SBF magnitudes. Figure 9 plots the "fluctuation color" $\overline{z}_{850}-\overline{H}_{160}$ as a function of broadband $(g_{475}-z_{850})$ and $(V-I)$ colors for these galaxies. The rms scatter of 0.21 mag in $\overline{z}_{850}-\overline{H}_{160}$ is consistent with measurement errors, and there is no evidence for a dependence on the broadband color. This implies that $\overline{H}_{160}$ will be extremely useful for future SBF studies when a modern, wide-area, space-based near-IR camera such as WFC3/IR becomes available. One cautionary note is that most of the galaxies in Figure 9 are fairly red, and the scatter in $\overline{H}_{160}$ shows evidence of increasing at bluer colors (Jensen et al. 2003). However, the prospects for $\overline{H}_{160}$ with WFC3/IR appear promising.
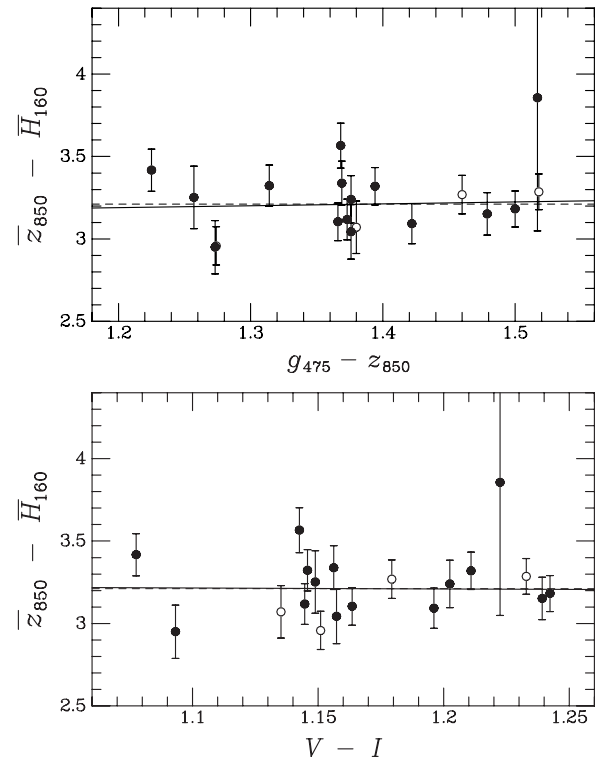
Figure 9. $\overline{z}_{850}-\overline{H}_{160}$ "fluctuation color" is plotted against $(g_{475}-z_{850})$ and $(V-I)$ photometric colors for galaxies having both ACS $\overline{z}_{850}$ and NICMOS $\overline{H}_{160}$ measurements (the latter from Jensen et al. 2003). Four Virgo galaxies (open circles) and 15 Fornax galaxies (filled circles) have both $\overline{z}_{850}$ and $\overline{H}_{160}$ data. The dashed line in each panel shows the weighted mean, while the solid line is the best-fitting linear relation. In both cases the slope is indistinguishable from zero, and the scatter is consistent with measurement errors. Thus, within observational limits, $\overline{z}_{850}$ and $\overline{H}_{160}$ have the same dependence on stellar population.

5.3. Structure of Fornax

Figure 10 shows the spatial distribution of the 43 ACSFCS galaxies plotted with their symbol sizes scaled inversely with SBF distance. The range of distances appears to increase slightly for galaxies farther away from the cluster center. This is not unexpected, since the highest density of galaxies will be near the center of the cluster, and the area is small, so there will be a lower incidence of galaxies projected from larger radii. The 21 galaxies at radii $r < 1°\!.5$ have an rms distance scatter of 0.080 mag, while the 22 at larger radii have an rms scatter of 0.105 mag. However, the significance of this difference is only $1.1\,\sigma$. Overall, the cluster appears compact with no obvious trends of distance with position. The two galaxies in our sample outside the FCC survey area, NGC 1340 and IC 2006, both have distances near the mean for the full sample.

The compact structure is further illustrated in Figure 11, which plots offset in line-of-sight distance versus projected physical distance in the R.A. and decl. directions from the central galaxy. As noted in the caption, there is a bias for the cluster to appear elongated along the line of sight in this figure, both because of distance measurement errors and selection effects in an area-limited survey. However, the central Mpc looks fairly symmetric. The rms dispersions in projected distance east–west and north–south of the cluster center are 0.52 ± 0.06 Mpc and 0.47 ± 0.06 Mpc, respectively, where the errors are estimated from bootstrap resampling. If we instead use robust biweight estimates, these become 0.52 ± 0.07 Mpc and 0.44 ± 0.08 Mpc, respectively, not sensibly different from the rms values.
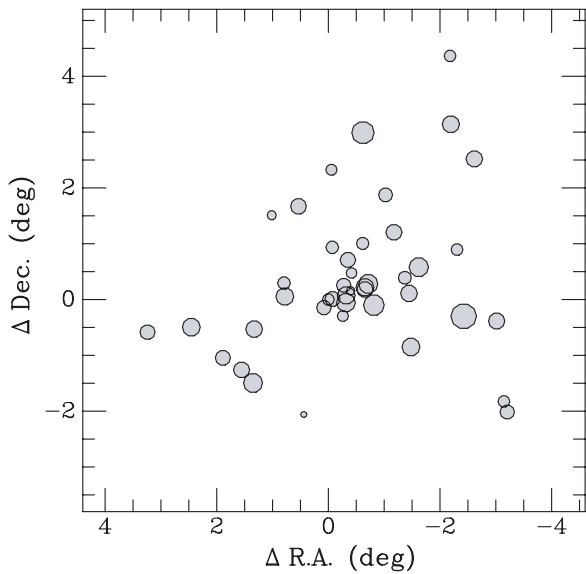
Figure 10. Spatial distribution of the ACS Fornax cluster galaxies. The offsets in right ascension and declination are computed with respect to the cD galaxy NGC 1399. This plot is similar to Figure 2 of Jordan et al. (2007), except here the point size is scaled inversely with the square of the SBF distance. The range in distance (point size) appears to increase with radius from the cluster center; for instance, the most distant galaxy FCC249 is also the farthest south, and the two nearest galaxies with $d < 19$ Mpc are both at radii $r > 2°$, well beyond the cluster core. However, there is no obvious trend of distance with position along any preferred axis.
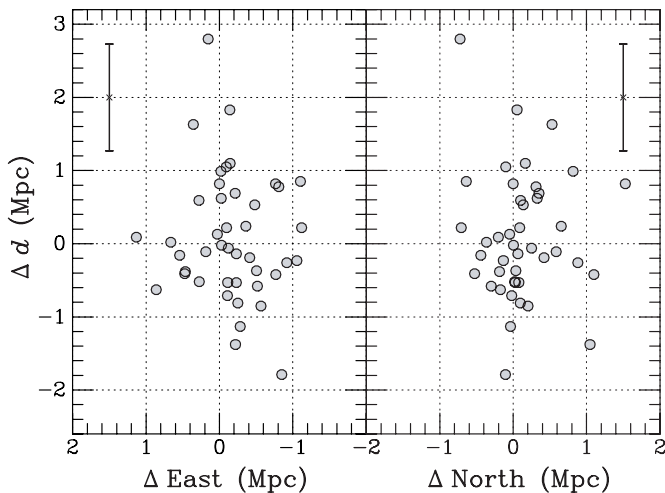
Figure 11. Galaxy distance (with respect to the mean of 20 Mpc) is plotted versus physical offset in Mpc east–west (left panel) and north–south (right panel) with respect to NGC 1399. Although different ranges are plotted along the horizontal and vertical axes, the scale is the same in both directions. The cluster appears fairly symmetric in the distance–R.A. plane (left) and somewhat narrower in the declination direction (right). However, this is mainly because of distance measurement errors; the median error in Δd is shown in each panel. There is a bias toward the cluster appearing elongated along the line of sight due to distance errors and because galaxies more than about ± 1.5 Mpc from the cluster mean would not be included in the FCC catalogue if the offset were in the plane of the sky rather than along the line of sight.

To estimate the true rms linear depth, we correct for the mean measurement error $\sigma_{err} = 0.047$ mag and the SBF method intrinsic scatter $\sigma_{cos} = 0.06 \pm 0.01$ mag, to obtain $\sigma_d = 0.49^{+0.11}_{-0.15}$ Mpc, where the quoted error bars are the 1σ uncertainties on the rms depth σ_d. The $\pm 2\sigma_d$ distance depth of Fornax is then $2.0^{+0.4}_{-0.6}$ Mpc. However, this estimate is somewhat circular because we used the spatial distribution on the sky to constrain
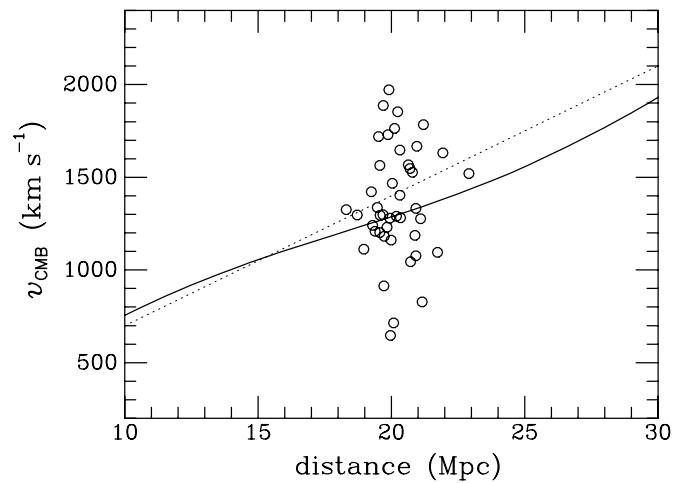
Figure 12. Hubble diagram for our 43 ACSFCS galaxies. The solid curve shows the velocity–distance relation along the Fornax line of sight as predicted by the *IRAS* galaxy density field (Blakeslee et al. 2002). The dotted line shows a pure Hubble flow for $H_0 = 70$ km s^{-1} Mpc^{-1}. As expected for a spatially compact, virialized structure, there is no relation between distance and velocity for this sample of early-type Fornax cluster galaxies.

the value of σ_{cos} in the χ^2 analysis of Section 4. For example, if we set $\sigma_{cos} = 0$, then the depth estimate increases to $0.74^{+0.15}_{-0.20}$ Mpc. This therefore sets a firm upper limit of $\sigma_d < 0.9$ Mpc on the rms depth of Fornax. Conversely, we can also force the depth to zero by setting $\sigma_{cos} \approx 0.08$ mag, which sets a limit on the intrinsic scatter of the z_{850}-band SBF method to be $\sigma_{cos} \lesssim 0.08$ mag. The compact nature of Fornax allows us to place firmer limits on σ_{cos} than did the Virgo cluster, where the rms depth in magnitudes is larger than the upper limit on σ_{cos}.

Figure 12 presents the velocity–distance relation for our sample of Fornax galaxies. In contrast to the results for Virgo from ACSVCS-XIII, we do not find evidence for nonvirial motions in our sample. Both the velocities and distances have much smaller ranges in Fornax than in Virgo, and we find no correlations between them in our limited sample. The cluster appears to be well virialized. Unlike Virgo or Centaurus, the two massive attractors that dominate the local velocity field (with likely a residual dipole due to more distant mass concentrations), Fornax has no surrounding supercluster. It was not detected as an attractor in the velocity field analysis by Tonry et al. (2000); their model χ^2 was not significantly improved by adding the additional parameters for a velocity attractor at the location of Fornax. Instead, that work simply assigned the Fornax cluster galaxies an increased velocity dispersion equal to about twice the background thermal dispersion, and about half that of Virgo.

However, the signature of the mass of Fornax is present in the velocity–distance curve inferred from the *IRAS* galaxy density field, and we show the relation for the Fornax line of sight from Blakeslee et al. (2002), which used $H_0 = 73$ km s^{-1} Mpc^{-1}. For comparison, the dotted line shows an unperturbed Hubble flow with $H_0 = 70$ km s^{-1} Mpc^{-1}. While it would be unwarranted to present a value for H_0 from a single nearby cluster, even with a highly accurate distance, the consistency of the mean distance and velocity within the accepted range of H_0 is reassuring.

We note that Dunn & Jerjen (2006) combined their sample of dwarf galaxy SBF distances with those of Jerjen (2003) and Ton01 and proposed that a composite sample of 29 early-type galaxies within $2°$ of NGC 1399 showed some evidence for the S-shaped signature of galaxy infall. This feature is not evident in the Ton01 data by itself. Further, Dunn & Jerjen noted that the

measurement accuracy was "not sufficient to establish the reality of the effect," and concluded that there was "no evidence for elongation along the cluster line of sight" even in the composite sample. However, their Figure 7 remains suggestive. It may be that the fainter Fornax dwarfs which constituted the Dunn & Jerjen samples (all but three of which are fainter than our sample magnitude limit) are preferentially infalling into the cluster. This is an intriguing possibility that deserves following up with high-precision *HST* SBF distances for a fainter sample of Fornax dwarfs.

5.4. Fluctuation Count $\overline{N}$ and an Alternative SBF Calibration

The absolute SBF magnitude $\overline{M}$ in a given bandpass has a corresponding "fluctuation luminosity" $\overline{L}$, which is equal to the luminosity-weighted mean luminosity of the stellar population in a galaxy (or star cluster, etc.). The ratio $L_{tot}/\overline{L}$ gives the total galaxy luminosity in units of $\overline{L}$, which depends on the stellar population and generally gets fainter for redder galaxies, as shown by the calibrations derived here and elsewhere. Viewed another way, this ratio represents the number of stars of luminosity $\overline{L}$ needed to constitute the luminosity of the galaxy. Motivated by these considerations, Ton01 introduced the distance-independent "fluctuation count" $\overline{N}$, defined in a given bandpass as

$$\overline{N} = \overline{m} - m_{tot} = +2.5 \log\left[\frac{L_{tot}}{\overline{L}}\right]. \qquad (9)$$

Besides being distance independent, $\overline{N}$ is also independent of Galactic extinction, or even photometric calibration error if $\overline{m}$ and m_{tot} are determined from the same imaging material. However, it correlates well with galaxy color, a consequence of the mass–metallicity relation for early-type galaxies, as discussed by Blakeslee et al. (2001b). Ton01 found that the scatter in the predicted value of $(V-I)$ at a given $\overline{N}_I$ was about 0.04 mag, based on a linear fit over the range $17 \lesssim \overline{N}_I \lesssim 23$.

Figure 13 shows the relation between $\overline{N}_z$ and $(g_{475}-z_{850})$ for the sample of 133 galaxies with SBF measurements from our Virgo and Fornax surveys. The total z_{850}-band magnitudes are from P. Côté et al. (2008, in preparation; see also ACSVCS-VI). These data cover a much larger range in luminosity $14.5 \lesssim \overline{N}_z \lesssim 22.5$ and stellar population. The range in $(g_{475}-z_{850})$ is more than twice the $(V-I)$ range used to define the $\overline{N}$ relation by Ton01, since that survey concentrated mainly on bright ellipticals and S0s. Our sample contains these galaxies as well, but is dominated by dwarfs, and we find that the relation between $(g_{475}-z_{850})$ and $\overline{N}_z$ is nonlinear for our full sample. It may be approximated by the simple least-squares linear and quadratic fits

$$(g_{475}-z_{850}) = 1.300 + 0.059\,(\overline{N}_z - 18), \qquad (10)$$

$$(g_{475}-z_{850}) = 1.327 + 0.060\,(\overline{N}_z - 18) - 0.0055\,(\overline{N}_z - 18)^2, \qquad (11)$$

which are plotted in Figure 13 and yield rms scatters in $(g_{475}-z_{850})$ of 0.083 and 0.079 mag, respectively. The scatter also increases at low $\overline{N}_z$ in a manner similar to that of standard galaxy color–magnitude diagrams.

The correlation of the distance-independent $\overline{N}_z$ with color means that it can be used to define an alternative SBF calibration, which may be useful especially in cases of large or uncertain
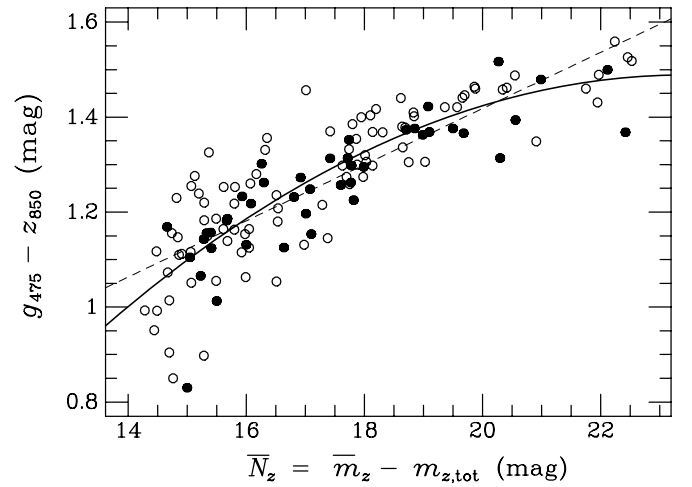
Figure 13. Galaxy $(g_{475}-z_{850})$ color is plotted as a function of the "fluctuation count" $\overline{N}_z$, the difference between the SBF magnitude $\overline{z}_{850}$ and the total z magnitude of the galaxy. The open and filled circles represent Virgo and Fornax galaxies, respectively. Note that $\overline{N}_z$, like $(g_{475}-z_{850})$, is independent of galaxy distance and can therefore be used as another means of calibrating the SBF distances, but unlike color, it is also independent of Galactic extinction. Ton01 showed that $\overline{N}_I$ scaled approximately linearly with $(V-I)$ over the range $16.5 < \overline{N}_I < 22.5$. Here, we extend the range by another two magnitudes; the resulting relation exhibits curvature at the blue/low-luminosity end. The dashed line shows the best-fit linear relation, while the solid curve is a quadratic fit.

Galactic extinction. Surprisingly, Blakeslee et al. (2002) found that the Ton01 SBF distances showed 25% less scatter when recalibrated using $\overline{N}_I$ instead of $(V-I)$ in a comparison to the peculiar velocity predictions from the *IRAS* galaxy density field. This was explained by the greatly reduced sensitivity to photometric measurement errors (a small error in $V-I$ would be amplified by a factor of 4.5 from the I-band SBF calibration) and Galactic extinction, an important consideration for an all-sky survey. In addition, the ground-based SBF galaxy sample was comparatively homogeneous in terms of galaxy type, with few if any dwarfs beyond the Local Group.

To test the usefulness of $\overline{N}$ for distance measurements, we repeated the same χ^2 analysis as in Section 4, except substituting $\overline{N}$ for $(g_{475}-z_{850})$. We find that the SBF calibration based on $\overline{N}_z$ is well described by a linear relation. Figure 14 shows the resulting $\overline{N}_z$ SBF calibration equivalent to Figure 5 for $(g_{475}-z_{850})$. In this case, the calibration no longer has a pure basis in stellar population properties, but rather brings in a scaling relation between galaxy luminosity and color. Therefore, any very luminous blue galaxy with recent star formation, or small red galaxy, perhaps tidally stripped like M32, should be expected to deviate from the relation. A particularly conspicuous outlier in this regard is the merger remnant NGC 1316 (FCC21), the brightest galaxy in Fornax. Its position near the extremum of the relation gives it a large influence on the slope; since it is a known outlier, we have removed it from the fit. However, it has little effect on the final relative distance modulus or internal scatter estimate, both of which change by less than 0.01 mag when it is included. We also label the two galaxies NGC 4486A (VCC1327) and NGC 4486B (VCC1297), which are close companions of M87 and have likely undergone tidal stripping. They would be expected to lie above the mean relation, and we find that this is indeed the case.

We use the same allowance for cluster depths as in the preceding section and find that a relative distance modulus of
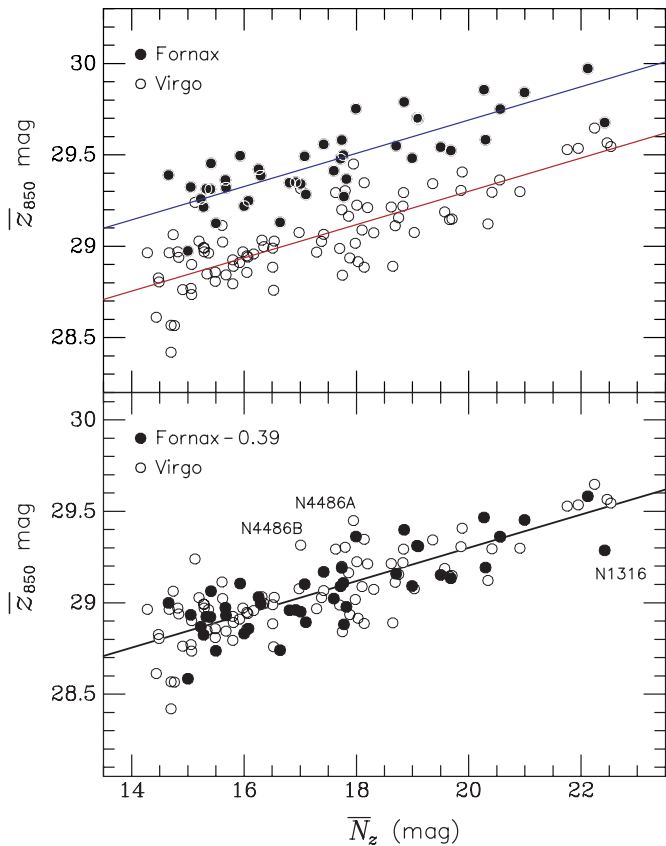
Figure 14. Alternative SBF calibration, similar to Figure 5, but $\overline{z}_{850}$ is here plotted as a function of $\overline{N}_z$. A linear fit provides an excellent description for this relation, although the estimated internal scatter is about 45% larger than the polynomial calibration against $(g_{475}-z_{850})$ color. The lower panel shows the two samples shifted together by subtracting the best-fit relative modulus $\Delta(m-M)_{\mathrm{FV}} = 0.39 \pm 0.03$ from the Fornax galaxy distance moduli. The very luminous, blue, post-merger galaxy FCC21 (NGC1316, labeled) is a prominent outlier and, because of its position at the bright end of the relation, has an undue influence on the slope; it has been omitted from the fit. The two M87 companion VCC1327 (NGC 4486A) and VCC1297 (NGC 4486B), which may be expected to deviate in the other sense from tidal stripping are also labeled.

(A color version of this figure is available in the online journal.)

$\Delta(m-M)_{\mathrm{FV}} = 0.39 \pm 0.03$ minimizes the value of χ^2. The best-fit relation is given by

$$\overline{M}_z = -1.98 + 0.089\,(\overline{N}_z - 18). \quad (12)$$

The magnitude zero-point differs from that in Equation (6) because $\overline{N} = 18$ does not correspond precisely to $(g_{475}-z_{850}) = 1.3$. Note that we can use the definition of $\overline{N}_z$ to rewrite this equation for the distance modulus:

$$(m-M) \approx 3.58 + 0.91\,\overline{z}_{850} + 0.09\,z_{850,\mathrm{tot}}, \quad (13)$$

where $z_{850,\mathrm{tot}}$ is the total apparent z_{850} magnitude of the galaxy. This shows that distances calculated from $\overline{N}_z$ are $\sim$9% less sensitive to the SBF $\overline{z}_{850}$ measurement errors and fairly insensitive to errors in the total magnitude. However, recall that this is all based on an empirical scaling relation. Ton01 cautioned that it may have systematic environmental or type dependences; both these effects are seen in Virgo for the closely related color–magnitude relation (Lisker et al. 2008).

In order to have $\chi^2_N = 1.0$, the $\overline{N}_z$ calibration in Equation (12) must have a cosmic scatter $\sigma_{\cos}(\overline{N}_z) \approx 0.10$ mag, which

is $\gtrsim 60\%$ larger than the intrinsic scatter for the calibration based on $(g_{475}-z_{850})$. Thus, we find that the SBF distances are more accurate when calibrated against color, in contrast to the ground-based data. This is likely because of the much higher precision of our measurements, which have errors smaller than the intrinsic scatter in the calibration relations, unlike the ground-based SBF data, where the measurement errors dominated. In addition, Galactic extinction is not a big issue here, since we are only dealing with two sightlines, both of which have minimal extinction. Further, our color calibration implies $\delta\overline{z}_{850}/\delta(g_{475}-z_{850}) \approx 1.5$, whereas the I-band calibration has slope $\delta\overline{I}/\delta(V-I) \approx 4.5$. Therefore, the ground-based I-band SBF distances are a factor of 3 more sensitive than ours to photometric errors in the color measurement. All of these factors contribute to the high precision of our $(g_{475}-z_{850})$-calibrated SBF distances; we prefer to adopt the relative distance modulus from that analysis, given its firm grounding in relatively well understood stellar population properties.

5.5. A Final Note on Virgo

Before concluding, we wish to note that our revised calibration and retabulated distances have no effect on the conclusions of ACSVCS-XIII regarding the structure of Virgo. The rms difference in the distance moduli between our recalibrated Virgo distances and those used for the analysis of ACSVCS-XIII is only 0.02 mag. Only three galaxies (the reddest ones) have moduli differing by more than 0.05 mag, in the sense of the recalibrated values being lower, and the maximum difference is 0.10 mag. None of these changes affect our earlier conclusions. However, we have presented the revised values in Table 2 in order to make the most homogeneous set of Virgo and Fornax galaxy distances, based on our final calibration for this project, readily available.

6. SUMMARY AND CONCLUSIONS

We have presented new SBF magnitude and color measurements for 43 galaxies observed in the ACSFCS. We first used these data to fit the variation of the apparent SBF magnitude $\overline{z}_{850}$ with galaxy $(g_{475}-z_{850})$ color based on the ACSFCS data alone. The relation is nonlinear, as found previously in ACSVCS-XIII. For a quadratic fit, the observed scatter in the Fornax $\overline{z}_{850}$ versus $(g_{475}-z_{850})$ relation is 0.092 mag. This contains contributions from measurement error ($\sim$0.047 mag), true distance variations within Fornax ($\sim$0.053 mag), and the cosmic scatter $\sigma_{\cos}$ in $\overline{M}_z$ at a given $(g_{475}-z_{850})$ due to stellar population effects ($\sim$0.060 mag). This is the first large SBF study in which measurement errors and depth effects are each smaller than the intrinsic scatter, affording us the opportunity for interesting constraints on $\sigma_{\cos}$. We determined $\sigma_{\cos} = 0.06 \pm 0.01$, with a firm upper limit $\sigma_{\cos} < 0.08$ mag, as this would require the cluster to have zero depth. This result holds for the combined Virgo+Fornax sample of galaxies with $(g_{475}-z_{850}) > 1.02$ mag. For the small number of bluer galaxies, mainly in Virgo, we estimate $\sigma_{\cos} \approx 0.13$ mag.

The combination of our Fornax SBF sample with that of Virgo from ACSVCS-XIII represents the largest homogeneous set of SBF measurements available, with nearly identical observing and data analysis procedures. The few modifications to the procedures were done in order to make the analysis more robust and automatic, and we have described them in detail. However, the Virgo galaxy selection extended to fainter luminosities, thus including a more significant blue tail of galaxies. Despite this,

the overall means of the galaxy color distributions are very similar. We used χ^2 minimization to fit a single polynomial calibration for $\overline{M}_z$ in terms of $(g_{475}-z_{850})$ for both Virgo and Fornax galaxies, assuming a range of relative distance moduli for the two clusters. Thus, we derived the following revised calibration, valid for $0.8 < (g_{475}-z_{850}) < 1.6$:

$$\overline{M}_z = (-2.04 \pm 0.15) + 1.41\,x + 2.60\,x^2 + 3.72\,x^3, \quad (14)$$

where $x \equiv (g_{475}-z_{850}) - 1.3$. The error on the $\overline{M}_z$ zero point comes from the total uncertainty in the Cepheid distance scale and the tie between spiral and early-type galaxy distances. The intrinsic scatter about Equation (14) is again 0.06 mag.

We have tabulated recalibrated distances for a total of 134 early-type galaxies from the two surveys and NGC 4697 in the Virgo Southern Extension. The calibration procedure determined a best-fit relative Fornax–Virgo distance modulus $\Delta(m-M)_{\rm FV} = 0.42\pm0.02$ mag, where the error bar $(1\,\sigma)$ comes from the χ^2 analysis and was verified by bootstrap resampling. This result is robust, regardless of whether or not the blue tail of galaxies is included in the fit: the full sample requires the cubic polynomial calibration above, whereas a quadratic suffices for $(g_{475}-z_{850}) > 1.02$ mag, but the best-fit relative distance is the same. After considering all possible systematic effects, we estimate the total uncertainty on $\Delta(m-M)_{\rm FV}$ is ±0.03 mag. For an adopted Virgo distance modulus of $(m-M)_{\rm Vir} = 31.09 \pm 0.15$ mag, the resulting Fornax modulus is $(m-M)_{\rm For} = 31.51\pm0.03\pm0.15$ mag, or a distance of $d_F = 20.0\pm0.3\pm1.4$ Mpc. The physical distance between the centers of Virgo (M87) and Fornax (NGC 1399) is then 33.4 ± 0.5 Mpc.

Correcting for measurement error and internal/cosmic scatter in the method, we estimate the rms line-of-sight depth of Fornax cluster to be $\sigma_d = 0.49^{+0.11}_{-0.15}$ Mpc. The total back-to-front depth of Fornax (i.e., $\pm2\sigma_d$) is therefore about $2.0^{+0.4}_{-0.6}$ Mpc, meaning that the cluster galaxies span a distance range of 19–21 Mpc. However, this estimate depends on our value of $\sigma_{\rm cos} = 0.06 \pm 0.01$ mag for the cosmic scatter. If we had unrealistically assumed $\sigma_{\rm cos} \equiv 0$ (i.e., SBF is a perfect distance indicator with no internal scatter), then the rms depth estimate would increase to $0.74^{+0.15}_{-0.20}$ Mpc; this provides an upper limit to the true rms depth of Fornax. We do not find any evidence for trends in the galaxy distances along any preferred direction on the sky, nor do we find evidence for nonvirial motions. In particular, there is no sign of ongoing cluster infall among the galaxies in our sample. It would be interesting to see if this also holds true for faint cluster dwarfs below our magnitude limit and later-type galaxies.

We compared our ACS Virgo and Fornax SBF measurements to the ground-based values of Ton01 for 50 galaxies in common. Our measurement errors are a factor of 3 smaller than those from the ground-based survey. Overall, the distances agree within the errors without any adjustments. We also compared our $\overline{z}_{850}$ measurements to the near-IR $\overline{H}_{160}$ data from Jensen et al. (2003) for 19 galaxies in common. The resulting SBF color $\overline{z}_{850}-\overline{H}_{160}$ exhibits a scatter consistent with measurement error and no dependence on the integrated galaxy color, although the sample is limited to fairly red galaxies. This suggests that $\overline{H}_{160}$ is capable of providing large samples of excellent SBF distances with less sensitivity to dust extinction, an important consideration for all-sky surveys.

The distance-independent fluctuation count $\overline{N} = \overline{m} - m_{\rm tot}$ scales logarithmically with the number of stars in a galaxy, and is therefore related to the total mass. It correlates with galaxy color

because of the mass–metallicity scaling relation. We presented linear and quadratic fitting functions for the dependence of $\overline{N}$ on $(g_{475}-z_{850})$ in the combined cluster sample. We then repeated the $\overline{M}_z$ calibration fit, but with $\overline{N}_z$ as the distance-independent parameter instead of $(g_{475}-z_{850})$. The resulting calibration is linear, but bright blue galaxies with recent star formation and small red galaxies that have undergone tidal stripping are expected, and observed, to be outliers. Further, the intrinsic scatter in the $\overline{M}_z$–$\overline{N}_z$ relation is 0.10 mag, or 2/3 larger than for the standard $\overline{M}_z$–$(g_{475}-z_{850})$ calibration, but the best-fit relative distance modulus of 0.39 ± 0.03 mag agrees with the result from the standard calibration. However, we prefer the relative distance from the $(g_{475}-z_{850})$ analysis because of its smaller scatter and pure basis in stellar population properties.

The ACS Virgo and Fornax cluster surveys have shown the power of the SBF method when coupled with an instrument such as ACS. In ACSVCS-XIII, we successfully mapped the three-dimensional structure of the Virgo cluster, and here we have determined a precise value for the relative distance of Fornax with respect to Virgo. Additional SBF studies with ACS data are nearing completion and will provide new insight into the sources of the Local Group motion (see Blakeslee & Barber DeGraaff 2008 for an example of these data). Future all-sky optical surveys reaching faint limits from the ground should provide large amounts of uniform quality imaging data for SBF measurements. At longer wavelengths, the comparison of ACS and NICMOS SBF data hints at the superb potential for near-IR SBF studies once a modern, space-based IR camera comparable to ACS becomes available. New wide-area IR detectors with excellent cosmetic properties now available at many ground-based observatories present further exciting opportunities for SBF distance and stellar population studies, as multiband optical/IR SBF data are relevant to such problems as AGB evolution and the UV excess in elliptical galaxies (e.g., Buzzoni & González-Lópezlira 2008). It will be interesting to see all the directions taken by SBF research in its second 20 years.

REFERENCES

Ajhar, E. A., Lauer, T. R., Tonry, J. L., Blakeslee, J. P., Dressler, A., Holtzman, J. A., & Postman, M. 1997, AJ, 114, 626
Ajhar, E. A., Tonry, J. L., Blakeslee, J. P., Riess, A. G., & Schmidt, B. P. 2001, ApJ, 559, 584
Barber DeGraaff, R., Blakeslee, J. P., Meurer, G. R., & Putman, M. E. 2007, ApJ, 671, 1624
Binggeli, B., Sandage, A., & Tammann, G.A. 1985, AJ, 90, 1681
Biscardi, I., Raimondo, G., Cantiello, M., & Brocato, E. 2008, ApJ, 678, 168
Blakeslee, J. P., Ajhar, E. A., & Tonry, J. L. 1999, in Post-*Hipparcos* Cosmic Candles, Vol. 237, ed. A. Heck & F. Caputo (Dordrecht: Kluwer), 181
Blakeslee, J. P., Anderson, K. R., Meurer, G. R., Benítez, N., & Magee, D. 2003, in ASP Conference Ser. Vol. 295, Astronomical Data Analysis Software and Systems XII, ed. H. E. Payne, R. I. Jedrzejewski, & R. N. Hook (San Francisco, CA: ASP), 257

Blakeslee, J. P., & Barber DeGraaff, R. 2008, AJ, 136, 2295
Blakeslee, J. P., Lucey, J. R., Barris, B. J., Hudson, M. J., & Tonry, J. L. 2001a, MNRAS, 327, 1004
Blakeslee, J. P., Lucey, J. R., Tonry, J. L., Hudson, M. J., Narayanan, V. K., & Barris, B. J. 2002, MNRAS, 330, 443
Blakeslee, J. P., & Tonry, J. L. 1995, ApJ, 442, 579
Blakeslee, J. P., & Tonry, J. L. 1996, ApJ, 465, L19
Blakeslee, J. P., Vazdekis, A., & Ajhar, E. A. 2001b, MNRAS, 320, 193
Bohlin, R. C. 2007, Instrument Science Report ACS-2007-006 (Baltimore, MD: STScI)
Bruzual, G., & Charlot, S. 2003, MNRAS, 344, 1000
Buzzoni, A., & González-López ira, R. A. 2008, ApJ, 686, 1007
Cantiello, M., Blakeslee, J., Raimondo, G., Brocato, E., & Capaccioli, M. 2007a, ApJ, 668, 130
Cantiello, M., Blakeslee, J. P., Raimondo, G., Mei, S., Brocato, E., & Capaccioli, M. 2005, ApJ, 634, 239
Cantiello, M., Raimondo, G., Blakeslee, J. P., Brocato, E., & Capaccioli, M. 2007b, ApJ, 662, 940
Cantiello, M., Raimondo, G., Brocato, E., & Capaccioli, M. 2003, AJ, 125, 2783
Cerviño, M., Luridiana, V., & Jamet, L. 2008, A&A, 491, 693
Côté, P., et al. 2004, ApJS, 153, 223 (ACSVCS I)
Côté, P., et al. 2007, ApJ, 671, 1456
Dunn, L. P., & Jerjen, H. 2006, AJ, 132, 1384
Ferguson, H. C. 1989, AJ, 98, 367
Ferrarese, L., et al. 2000, ApJ, 529, 745
Ferrarese, L., et al. 2006, ApJS, 164, 334 (ACSVCS-VI)
Freedman, W. L., et al. 2001, ApJ, 553, 47
Fruchter, A. S., & Hook, R. N. 2002, PASP, 114, 144
González, R. A., Liu, M. C., & Bruzual, A. G. 2004, ApJ, 611, 270
González-López ira, R. A., Albarrán, M. Y., Mouhcine, M., Liu, M. C., Bruzual, A. G., & de Batz, B. 2005, MNRAS, 363, 1279
Jacoby, G. H., et al. 1992, PASP, 104, 599
Jensen, J. B., Tonry, J. L., Barris, B. J., Thompson, R. I., Liu, M. C., Rieke, M. J., Ajhar, E. A., & Blakeslee, J. P. 2003, ApJ, 583, 712
Jensen, J. B., Tonry, J. L., & Luppino, G. A. 1998, ApJ, 505, 111
Jensen, J. B., Tonry, J. L., Thompson, R. I., Ajhar, E. A., Lauer, T. R., Rieke, M. J., Postman, M., & Liu, M. C. 2001, ApJ, 550, 503
Jerjen, H. 2003, A&A, 398, 63
Jerjen, H., Binggeli, B., & Barazza, F. D. 2004, AJ, 127, 771
Jordán, A., et al. 2004, ApJS, 154, 509 (ACSVCS II)
Jordán, A., et al. 2005, ApJ, 634, 1002 (ACSVCS-X)
Jordán, A., et al. 2007, ApJS, 169, 213 (ACSFCS-I)

Kelson, D. D., et al. 2000, ApJ, 529, 768
Koekemoer, A. M., Fruchter, A. S., Hook, R. N., & Hack, W. 2002, in Proc. The 2002 *HST* Calibration Workshop: Hubble after the Installation of the ACS and the NICMOS Cooling System, ed. S. Arribas, A. Koekemoer, & B. Whitmore (Baltimore, MD: STScI), 337
Landolt, A. U. 1992, AJ, 104, 340
Lee, H.-C., Worthey, G., & Blakeslee, J. P. 2007, in Proc. IAU Symp. 241, Stellar Populations as Building Blocks of Galaxies, ed. A. Vazdekis, R. F. Peletier (Cambridge: Cambridge Univ. Press), 187
Lisker, T., Grebel, E. K., & Binggeli, B. 2008, AJ, 135, 380
Liu, M. C., Charlot, S., & Graham, J. R. 2000, ApJ, 543, 644
Liu, M. C., Graham, J. R., & Charlot, S. 2002, ApJ, 564, 216
Macri, L. M., Stanek, K. Z., Bersier, D., Greenhill, L. J., & Reid, M. J. 2006, ApJ, 652, 1133
Madore, B. F., et al. 1998, Nature, 395, 47
Marín-Franch, A., & Aparicio, A. 2006, A&A, 450, 979
Mei, S., Quinn, P. J., & Silva, D. R. 2001, A&A, 371, 779
Mei, S., Scodeggio, M., Silva, D. R., & Quinn, P. J. 2003, A&A, 399, 441
Mei, S., et al. 2005a, ApJS, 156, 113 (ACSVCS IV)
Mei, S., et al. 2005b, ApJ, 625, 121 (ACSVCS-V)
Mei, S., et al. 2007, ApJ, 655, 144 (ACSVCS-XIII)
Mieske, S., Hilker, M., & Infante, L. 2003, A&A, 403, 43
Mieske, S., Hilker, M., & Infante, L. 2006, A&A, 458, 1013
Mouhcine, M., González, R. A., & Liu, M. C. 2005, MNRAS, 362, 1208
Neilsen, E. H., & Tsvetanov, Z. I., Jr. 2000, ApJ, 536, 255
Pahre, M. A., et al. 1999, ApJ, 515, 79
Press, W. H., Teukolsky, S. A., Vetterling, W. T., & Flannery, B. P. 1992, in Numerical Recipes in FORTRAN. The Art of Scientific Computing (2nd ed.; Cambridge: Cambridge Univ. Press)
Raimondo, G., Brocato, E., Cantiello, M., & Capaccioli, M. 2005, AJ, 130, 2625
Riess, A. 2004, Instrument Science Report ACS-2004-017 (Baltimore, MD: STScI)
Schlegel, D. J., Finkbeiner, D. P., & Davis, M. 1998, ApJ, 500, 525
Sirianni, M., et al. 2005, PASP, 117, 1049
Tonry, J. L. 1991, ApJ, 373, L1
Tonry, J. L., Ajhar, E. A., & Luppino, G. A. 1990, AJ, 100, 1416
Tonry, J. L., Blakeslee, J. P., Ajhar, E. A., & Dressler, A. 1997, ApJ, 475, 399
Tonry, J. L., Blakeslee, J. P., Ajhar, E. A., & Dressler, A. 2000, ApJ, 530, 625
Tonry, J. L., Dressler, A., Blakeslee, J. P., Ajhar, E. A., Fletcher, A. B., Luppino, G. A., Metzger, M. R., & Moore, C. B. 2001, ApJ, 546, 681 (Ton01)
Tonry, J. L., & Schneider, D. P. 1988, AJ, 96, 807
Tully, R. B. 1982, ApJ, 257, 389